Upscaling and Scale Effects

Marco Dentz, Jesus Carrera, and Juan Hidalgo

May 25, 2016

Contents

4.1 Scale Effects

The basic issue with upscaling may be illustrated with an example from Bronstert et al. (2005). Watching a movie of boats in the ocean, alert spectators immediately and intuitively identify whether the boats were filmed in a pool or in the actual ocean.

Pool waves may look as large as ocean ones, but they never look as foamy. The reason is that surface tension, which is an important force for small water bodies, becomes negligible when compared the inertial forces of true ocean waves. While it is evident that dominant processes may change with scale, the conventional continuum mechanics approach does not acknowledge it. The continuum mechanics approach is sound as long as the main processes remain unaltered. However, one of the points of this Chapter is that such is rarely, if ever, the case for the processes involved in geological CO_2 storage. Variability is important not only because of the associated uncertainty, but also because large-scale behaviour of a spatially variable phenomenon may be significantly different from the small-scale behaviour. This means, changes in scale may (1) lead to changes in the effective parameters, (2) cause new processes to emerge, which often will imply (3) that the governing equations need to be changed. The term *scale effect* refers to any of these changes. Upscaling is a general term that refers to the procedures to derive these changes (in parameters, relevant processes, or governing equations) assuming that parameters, processes, and governing equations ar known at a small scale. This Chapter is motivated by the recognition that spatial and temporal variability is (1) very important, and (2) impossible to describe in detail. Therefore, scale effects should be expected in general.

Processes involved in CO_2 storage include: single and multiphase flow, solute transport, energy transport, chemical reactions and mechanical deformations. All of them suffer from scale effects. Single phase flow is governed by the flow equation, which basically entails fluid mass and momentum conservation. The latter is expressed by Darcy's law, whose only parameter is hydraulic conductivity. While the flow equation is broadly accepted, it is also well known that hydraulic conductivity displays significant scale effects, that is, its representative value grows with the size of the problem (Renard and de Marsily, 1997; Sanchez-Vila et al., 2006). This implies that the hydraulic conductivity measured at one scale need not be equal to those described at

a different, larger scale. Since measurements are often made at small scales (e.g., cm or m), whereas flow may be need at much larger (e.g., 10^2 - 10^3 m) scales, it is clear that upscaling is important.

The situation is more complex for transport. Traditionally continuum scale transport through homogeneous media has been represented by the diffusion-advection equation (ADE) (Bear, 1972):

$$\phi \frac{\partial c(\mathbf{x}, t)}{\partial t} + \mathbf{q} \cdot \nabla c(\mathbf{x}, t) - D \nabla^2 c(\mathbf{x}, t) = 0, \tag{4.1}$$

where ϕ is porosity, $c(\mathbf{x}, t)$ represents the magnitude being transported per unit volume of fluid (e.g., concentration), $\mathbf{q}$ is the mean flux and D is the diffusion (dispersion) coefficient, which represents mixing caused by Brownian motion (or by fluctuations of the pore-scale fluid velocity around its mean).

Observed chemical transport in heterogeneous media does not behave as implied by (4.1) (e.g., Adams and Gelhar, 1992; Neuman and Zhang, 1990; Carrera, 1993; Berkowitz and Scher, 1997; Steefel et al., 2005). For one thing both apparent dispersivity (Lallemand-Barres and Peaudecerf, 1978; Gelhar et al., 1992) and porosity (Guimerà and Carrera, 2000) display marked scale effects. Dispersivity grows (almost) linearly with the scale of the problem, whereas porosity in fractured media grows with residence time. Differences are not restricted to transport parameters. Field observations differ from model predictions. It is therefore clear that the ADE is not adequate for simulating transport. A number of alternatives have been proposed in recent years. They will be discussed in Section 4.3. However, the driving force in the most recent developments has been reactive transport. When dealing with reactive transport, it is convenient to distinguish between fast reactions, which tend to proceed in equilibrium, and slow reactions, whose rate depends on the distance to equilibrium, as quantified by saturation.

Rezaei et al. (2005) showed that the actual rate of equilibrium reactions in porous media is controlled by mixing. The interplay between transport and chemistry is non

trivial. Specifically, performing geochemical calculations is needed, but does not suffice to predict where equilibrium reactions will take place, what will be their rate, or under which conditions will this rate be maximum. These outcomes are controlled by mixing. In fact, shortly thereafter, De Simoni et al. (2005) found a relatively simple expression to quantify mixing for Fickian dispersion. A result from these and many other works is that proper representation of reactive transport requires a proper representation of mixing. The large-scale ADE equates spreading and mixing in form of macrodispersion coefficients. While for a fluid at rest, or a hypothetical homogeneous porous medium, a diffusion or dispersion coeffcient is an operational concept to quantify solute mixing, this is very different for transport in heterogeneous flow fields, as illustrated in Figure 4.1. At practically relevant times, the macrodispersion concept quantifies the extension of the plume as opposed to the volume that is occupied by the solute as a consequence of mixing (Kitanidis, 1994; Dentz et al., 2000). Thus, the ADE parameterized by a (temporally evolving) macrodispersion coefficient quantifies rather the extension of the plume than mixing, and is therefore not suited for the quantification of reactive transport.

One might argue that slow reactions, whose rate is controlled by local chemistry, should not suffer from scale effects. As it turns out, kinetic reaction rates observed in the field are much slower than what might be expected from laboratory measurements (White and Peterson, 1990). This implies that local concentrations are not well represented in the ADE either (Lichtner and Kang, 2007). In fact, most of the alternatives to the ADE discussed in in this chapter adopt non local formalisms. That is, transport processes at one point in space and time depend not only on the concentration field at that point, but also on its spatial variability far away and on its time history.

We find similar scale effects in for the description of multiphase in heterogeneous porous media. This may manifest on one hand, in scale effects in effective flow parame-

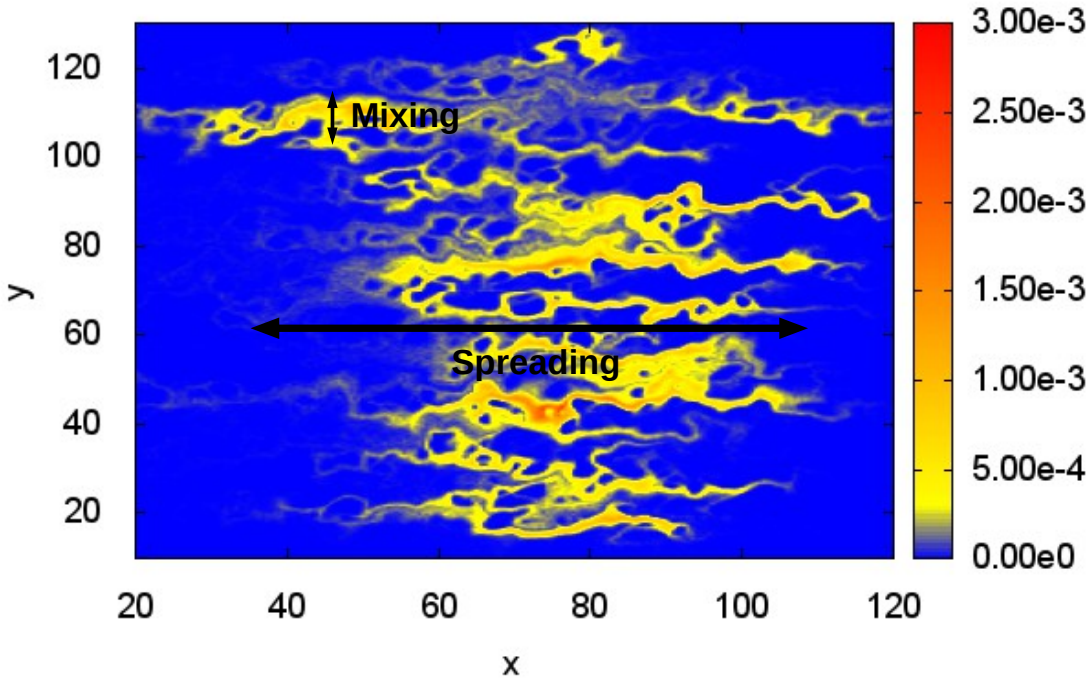

Figure 4.1: Mixing refers to the rate at which different waters blend together. As such, it is controlled by local gradients and tends to destroy local irregularities in concentration. Spreading, on the other hand, tends to increase the extent of the plume or the overall width of an advancing front. They are linked, because irregular spreading tends to generate gradients perpendicular to the flow direction, but they are different concepts. Yet, both are equated in the ADE.

ters such as intrinsic hydraulic conductivity, or scale effects in constitutive relationships such as capillary pressure saturation relations and relative permeability (Yang et al., 2013). On the other hand, heterogeneity effects the spreading of a displacement in a way similar as observed in the case of the miscible displacement of one fluid by the other, which can be described by the single phase flow macrodispersion coefficient described above. For two-phase flow the phenomenon is analogous (Langlo and Espedal, 1995; Neuweiler et al., 2003; Bolster et al., 2009). Remarkably, for two-phase flow, this gives rise to a macrodispersive flux in the saturation equations for the two fluids. For

highly heterogeneous porous media, one observes similar fluid retention phenomena as for solute transport in multicontinuum media (Di Donato et al., 2007; Geiger et al., 2013).

In all these applications, scale effects are caused by the interaction of spatial heterogeneity and the small scale flow and transport processes, which can be seen as collective phenomena that may be described by effective parameters, or require the constitution of flow and transport equations that are different from the ones on the local scale. In the following, we gives an description of various efforts to approach the upscaling problem, and quantify large scale flow and transport in heterogeneous porous formations. This description needs to be necessarily incomplete due to the vast amount of literature that has been dedicated to this important topic in the last 50 years.

4.2 Single Phase Flow

The following sections describe the upscaling of porous media flow from the pore to Darcy scale, and from the Darcy to the field scale.

4.2.1 Pore to Darcy Scale

On the pore scale, the medium is composed of void space that is available to the fluid and a solid phase that here is assume to be impermeable. Figure 4.2 shows a X-ray microtomography cross section of the heterogeneous pore-structure of a pure calcite limestone. In the following, we briefly introduce into the description of single phase flow on this scale, and its upscaling to the continuum or Darcy scale, which is assumed to be much larger than a typical pore lenght scale.

The pore space available for fluid flow is denoted by Ω_f, the solid space by Ω_s. Their boundaries are denoted by $\partial\Omega_f$ and $\partial\Omega_s$. The space occupied by the bulk of the porous medium is denoted by $\Omega = \Omega_f \cup \Omega_s$. The solid grains are assumed to be

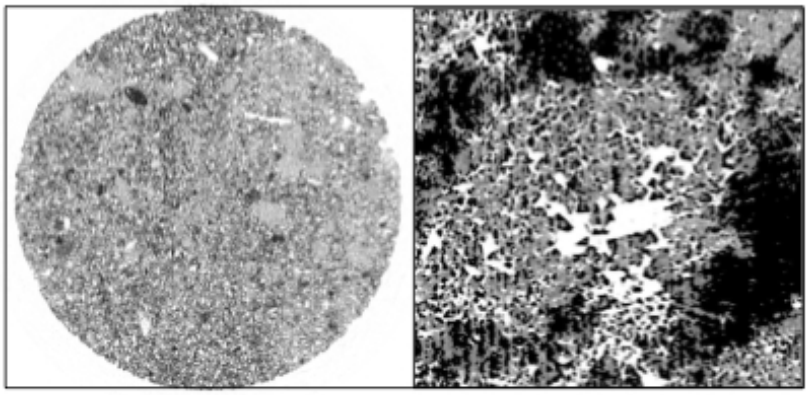

Figure 4.2: X-ray microtomography cross section of a pure calcite limestone imaged at different resolutions. Left, porosity map (diameter 1 cm; resolution $5\mu m$). Right, processed image (600×600 μm, resolution $1\mu m$) showing the mobile domain (in white) and the micro-porosity distribution in the immobile domain formed by clusters of distinctly different size (grey scale). Zones in black are areas unconnected with the immobile domain (porosity lower than the percolation threshold, see also Gouze et al. (2008).

impermeable. Flow in the pore space is governed by the Navier-Stokes equation

$$\rho_f \frac{\partial \mathbf{v}(\mathbf{x},t)}{\partial t} + \mathbf{v}(\mathbf{x},t) \cdot \nabla \mathbf{v}(\mathbf{x},t) = \mu \nabla^2 \mathbf{v}(\mathbf{x},t) - \nabla p(\mathbf{x},t) + \rho_f g, \tag{4.2}$$

where ρ_f is the fluid density, $\mathbf{v}(\mathbf{x},t)$ is the fluid velocity, μ is dynamic viscosity, $p(\mathbf{x},t)$ is fluid pressure and g is the gravity acceleration. The first two terms on the left describe fluid acceleration, the first two terms on the right quantify the action of shear and stress on a fluid volume in terms of pressure (stress) and viscosity (shear), the last term quantifies body forces, which here is only the action of gravity.

Flow can be characterized by the dimensionless Reynolds number $Re = \ell v_c / \nu$ with ℓ a characteristic pore length scale, v_c a characteristic flow rate, and $\nu = \mu/\rho$ kinematic viscosity. The Reynolds number compares fluid inertia (ℓv_c) to vicous resistance (ν). We assume that the fluid density is constant, which means that we focus on isothermal flow that is not affected by solute transport. Furthermore, for $Re \ll 1$ as is typically the case for porous media flows, inertia effects can be disregarded and thus, the Navier-

Stokes equation simplifies to the Stokes equation

$$\rho_f \frac{\partial \mathbf{v}(\mathbf{x},t)}{\partial t} = \mu \nabla^2 \mathbf{v}(\mathbf{x}) - \nabla p(\mathbf{x}) + \rho_f \mathbf{g}, \tag{4.3}$$

where $\mathbf{v}(\mathbf{x})$ is the pore velocity, μ is the fluid viscosity and $p(\mathbf{x})$ the fluid pressure, ρ_f is the fluid density and $\mathbf{g}$ is gravity acceleration. Since we assume that the fluid density is constant in time and space, fluid mass conservation implies $\nabla \cdot \mathbf{v}(\mathbf{x}) = 0$.

There are a series of approaches to solve the pore scale flow problem including Lattice-Boltzmann (e.g., Kang et al., 2006; Willingham et al., 2008; Acharya et al., 2007), smoothed particle hydrodynamics (e.g., Tartakovsky et al., 2007, 2009), computational fluid dynamics and pore network modeling (Meile and Tuncay, 2006; Li et al., 2006), see also the recent review by Meakin and Tartakovsky (2009). In general these methods are computationally very costly and therefore often limited to relatively small flow domains or relatively simple pore geometries. If we are interested in the global fluxes, it is not necessary to know all the small scale details of the fluctuations of $\mathbf{v}(\mathbf{x},t)$, but sufficient to determine the average fluid flow in a representative elementary volume (REV) V_r of the medium,

$$\mathbf{q}(\mathbf{x},t) = \frac{1}{V_r} \int\limits_{V_r} d\mathbf{r} \mathbf{v}(\mathbf{x}+\mathbf{r},t). \tag{4.4}$$

In order to illustrate the concept of the representative elementary volume, we consider the definition of porosity as done in the textbook by Bear (1972). Thus, we consider the volume of void space in a radius ℓ about a point $\mathbf{x}$,

$$V_f(\mathbf{x},\ell) = \int\limits_{V(\ell)} d\mathbf{r} \mathbb{I}(\mathbf{x}+\mathbf{r} \in \Omega_f), \tag{4.5}$$

where the indicator function $\mathbb{I}(\mathbf{r} \in \Omega_f)$ is 1 if the statement in its argument is true and 0 else, $V(\ell)$ is the bulk volume on the scale ℓ. The ratio $V_f(\ell)/V(\ell)$ fluctuates on a scale of the order of the pore diameter for small ℓ, where voids and grain are clearly distinguishable. For increasing scale ℓ, i.e., for ℓ larger than the characteristic pore

size, this ratio converges to the constant volumetric porosity. The scale ℓ_r at which this transition happens defines the representative elementary volume $V_r = V(\ell_r)$. Notice that this concept requires that the pore space can be characterized by a characterstic length scale. This concept does not apply for media characterized by fractal pore size distributions because of the lack of a characteristic pore size.

The Stokes equation (4.3) can be upscaled, or averaged using the methods of Homogenization and volume averaging (e.g., Whitaker, 1986; Bear, 1972; Hornung, 1997), for example. The average flow velocity $\mathbf{q}(\mathbf{x}, t)$ then satisfies the equation (e.g., Bear, 1972)

$$\mathbf{q}(\mathbf{x}, t) + \frac{\rho_f \mathbf{k}}{\phi\mu} \frac{\partial \mathbf{q}(\mathbf{x}, t)}{\partial t} - \frac{\mu^2 \mathbf{k}}{\mu} \nabla \mathbf{q}(\mathbf{x}, t) = -\frac{\rho_f g \mathbf{k}}{\mu} \nabla h(\mathbf{x}, t), \tag{4.6}$$

where the permeability tensor $\mathbf{k}$ reflects the medium geometry and composition, μ^e is an effective viscosity. The hydraulic head is defined by $h(\mathbf{x}, t) = p(\mathbf{x}, t)/(\rho_f g) + z$, the porosity ϕ compares the pore volume to the bulk volume of the porous medium, $\phi = V_f/V$. The first terms on the left hand side comes from the visous term in (4.3), the second from the acceleration term. The third term represents shear losses at the fluid grain interfaces and was introduced by Brinkman (1949). The term on the right side summarizes pressure and body forces. Under certain conditions the evolution equation for $\mathbf{q}(\mathbf{x}, t)$ may include memory terms that are non-local in time (e.g., Hornung, 1997). Fluid acceleration typically occurs on such small time scales that the transient term in (4.6) can be disregarded. Also the so-called Brinkman term can typically be neglected, which gives the Darcy equation

$$\mathbf{q}(\mathbf{x}, t) = -\mathbf{K} \nabla h(\mathbf{x}, t), \qquad \mathbf{K} = \frac{\rho_f g \mathbf{k}}{\mu}, \tag{4.7}$$

where $\mathbf{K}$ is hydraulic conductivity. Conductivity $\mathbf{K}$ is not only a property of the porous medium, but through its dependence on fluid density and viscosity also of the fluid. Notice that it also depends on gravity acceleration g which makes it a characteristic of the planetary conditions.

Fluid mass conservation for a Darcy scale porous medium finally is expressed by the continuity equation (Bear, 1972)

$$S_0 \frac{\partial h(\mathbf{x}, t)}{\partial t} + \nabla \cdot [\mathbf{K} \nabla h(\mathbf{x}, t)] = f(\mathbf{x}, t), \tag{4.8}$$

where $f(\mathbf{x}, t)$ represents the presence of volume sinks and sources. The specific volumetric storage $S_0 = \rho g[\alpha(1 - \phi) + \beta\phi]$ expresses the compressibility of the medium through α and of the fluid through β. It quantifies the volume of water that is released from a unit volume of aquifer per unit decline in hydraulic head $h(\mathbf{x}, t)$. In the following, we will assume that the hydraulic conductivity tensor is diagonal and isotropic such the $K_{ij} = K\delta_{ij}$.

Under the Dupuit assumption of predominantly horizontal flow, i.e., $h(\mathbf{x}, t) = h(x, y, t)$, the integration of the flow equation over the thickness d_a of the aquifer gives (Bear, 1972)

$$S \frac{\partial h(x, y, t)}{\partial t} + T \nabla^2 h(x, y, t) = F_v(x, y, t) + F_s(x, y, t), \tag{4.9}$$

where storativity $S = S_0 d_a$, transmissivity $T = K d_a$, $F_v(x, y, t)$ are the vertically integrated volume sources and sinks, and $F_s(x, y, t)$ are surface sources and sinks at the horizontal aquifer boundaries.

In the following we denote the Darcy scale also as continuum scale because it does not distinguish between solid grains and void space, but characterizes the physical medium properties in terms of the effective parameters hydraulic conductivity $\mathbf{K}$, porosity ϕ and specific volumetric storage S_0.

4.2.2 Darcy to Field Scale

The continuum-scale physical medium properties as quantified by the hydraulic conductivity K, porosity ϕ and specific storativity S_0 are in general spatially variable due to heterogeneity in the porous material. Hydraulic conductivity varies by 13 order of magnitude between different materials (Bear, 1972). Variability in porosity and specific storage is typically much lower.

This spatial variability leads to large-scale flow behaviors that are quantitatively different from the ones observed at a local scale, where the medium can be assumed to be homogeneous. The local scale refers to a length scale that is shorter than the characteristic variability scale of the medium. The Darcy equation (4.7) and the mass conservation equation (4.8) in a heterogeneous medium are given by

$$\mathbf{q}(\mathbf{x},t) = -K(\mathbf{x})\nabla h(\mathbf{x},t) \tag{4.10}$$

$$S_0(\mathbf{x})\frac{\partial h(\mathbf{x},t)}{\partial t} - \nabla \cdot \mathbf{q}(\mathbf{x},t) = f(\mathbf{x},t). \tag{4.11}$$

The detailed knowledge of the spatial variability of the physical medium properties in terms of $K(\mathbf{x})$ and $S_0(\mathbf{x})$, and the (numerical) solution of the local scale flow problem (4.11), can in principle quantify the observed flow behavior. However, the detailed characterization of the local scale medium fluctuations is in many practical applications not possible and also not desireable. As pointed out above for the upscaling from pore to Darcy scale, the characterization of large scale features of fluid flow does not require the detailed knowledge of the full local scale fluctuation behavior. Thus, coarse grained, averaged flow descriptions are required to quantify and explain observed large scale phenomena and to make predictions. As for the transition from the pore to the continuum scale discussed in the previous section, coarse graining and upscaling implies averaging of the Darcy equation (4.10).

In this context we distinguish between equilibrium and non-equilibrium approaches. Equilibrium approaches assume that large scale flow can be characterized by the Darcy equation characterized by an effective hydraulic conductivity. We call this an equilibrium approach because it assumes that flow at a coarse grained position $\mathbf{x}$ can be characterized by a single average value of hydraulic head. Non-equilibrium approaches average the flow equation (4.11) and arrive at flow equations that are characterized by memory kernels, which account for the fact that the support scale of the coarse flow description is not in local equilibrium.

In the following, we present approaches for the upscaling of the flow problem from

Darcy to field scale. We focus hereby on the scale dependence of hydraulic conductivity (Renard and de Marsily, 1997; Sanchez-Vila et al., 2006), as well as non-equilibrium approaches for fluid flow in media with large parameter contrasts.

4.2.2.1 Steady Flow: Effective Hydraulic Conductivity

The characterization of large scale flow in terms of effective hydraulic conductivity assumes that an average Darcy flow velocity $\mathbf{q}(\mathbf{x})$ on the large scale obeys the Darcy law

$$\overline{\mathbf{q}}(\mathbf{x}) = -\mathbf{K}^e \nabla \overline{h}(\mathbf{x}), \tag{4.12}$$

where the effective hydraulic conductivity tensor $\mathbf{K}^e$ measures the average flux subject to a unit gradient of an average hydraulic conductivity $\overline{h}(\mathbf{x}, t)$. Equation (4.12) defines the effective hydraulic conductivity, which, in general, is a tensorial quantity. Directional dependence of large scale conductivity can be due to statistical anisotropy of the local hydraulic conductivity distribution, boundary distributions, or due to the domain geometry. Exact results for the effective hydraulic conductivity exist only for layered media, and two-dimensional porous media whose conductivities satisfy certain conditions.

Stratified Media A heterogeneous porous medium whose conductivity values are organized in strata of equal thickness d and thus depend only on the z-direction, $K(\mathbf{x}) = K(z)$. The medium can be characterized by the sequence of conductivity values $\{K_n\}$ in the strata, where the subscript n determines the spatial position within the medium. We consider the case of steady flow characterized by $\nabla \cdot \mathbf{q}(\mathbf{x}) = 0$.

Let us consider now the effective flow behavior in such a medium. First, we consider flow in z–direction, perpendicular to the direction of stratification, which implies that flow is aligned with the direction perpendicular to the stratification. The flow equation (4.11) now becomes $\frac{\partial}{\partial z} K(z) \frac{\partial h(z,t)}{\partial z} = 0$. The solution for hydraulic conductivity for constant head boundary conditions is given by integration

as $h(z) = h_0 - K_H G \int_0^z dz' q/K(z')$, where $G = \frac{\partial \overline{h}(z)}{\partial z} = (h_w - h_0)/L$ is the large scale hydraulic gradient, h_0 and h_w are the hydraulic heads at inlet and outlet; the vertical extension of the domain is $w = Nd$; $K_H = (w/d)(\sum_n K_n^{-1})^{-1}$ is the harmonic average of the specific sequence of conductivity values. The Darcy equation can now be written in terms of the global hydraulic head $\overline{h}(z)$ and K_H as

$$q = -K_H \frac{\partial \overline{h}(z)}{\partial z}. \tag{4.13}$$

Notice that the flow problem is completely defined by the global hydraulic gradient and the harmonic mean of the conductivity values within the flow domain. Details such as the exact sequence $\{K_n\}$ do not play a role.

We consider now flow in x–direction, aligned with the direction of stratification. In this case, the flow equation (4.11) becomes $\frac{\partial}{\partial x} K(z) \frac{\partial h(x,t)}{\partial x} = 0$. For constant head boundary conditions at $x = 0$ and $x = L$, the solution for the hydraulic head is independent of the z-direction. Thus the Darcy equation reads as $q(z) = -K(z)\partial h(x)/\partial x$, and we obtain for the global flow $\overline{q} = w^{-1} \int_0^w dz q(z)$ the effective Darcy equation

$$\overline{q} = -K_A \frac{\partial h(x)}{\partial x}, \tag{4.14}$$

where $K_A = (d/w) \sum_n K_n$ is the arithmetic mean over the values in the conductivity sequence $\{K_n\}$. Again, the details of the sequence are not of importance.

Stochastic Modeling The stochastic modeling approach interprets this sequence as a stochastic process in space. This means the conductivities K_n that form the sequence $\{K_n\}$ are assumed to be random variables characterized by a certain distribution $p_K(K)$. The stochastic process, i.e., the random sequence $\{K_n\}$ is characterized by the joint distribution of conductivity values K_n. Notice that each realization of this stochastic process, this means, each random sequence of conductivity values, defines an aquifer realization. In many geological media, the distribution of hydraulic conductivity $p_K(K)$ is found to follow approximately a log-normal distribution (Renard and de Marsily, 1997; Sanchez-Vila et al., 2006). In fact, the sequence $\{K_n\}$

is typically modeled as a multi-lognormally distributed stochastic process, which implies that $\{Y_n = \ln(K_n)\}$ is a multi-Gaussian distributed stochastic process. This means that the joint distribution of the Y_n is a multi-Gaussian distribution. Thus, the stochastic process $\{Y_n\}$ can be characterized by its mean $\overline{Y_n}$ and covariance function $\overline{(Y_i - \overline{Y_i})(Y_j - \overline{Y_j})} = C_{Y,ij}$. It is typically assumed that the process is stationary, which implies that the mean $\overline{Y_n} = \overline{Y}$, i.e., it does not depend on the position within the medium, and that the covariance $C_{Y,ij} = C_{Y,i-j}$, i.e., it depends only on the relative distance between the strata. The variance of log-conductivity is given by $\sigma_Y^2 = C_{Y,ii}$. Processes with this property are termed stationary processes.

The stochastic modeling approach substitutes now the spatial harmonic and arithmetic averages by their respective ensemble averages $\overline{K}_H = (\overline{1/K})^{-1}$ and $\overline{K}_A = \overline{K}$. The spatial and ensemble average quantities are in general not equal. The spatial average K_A is in general an average over a finite number of strata, while the stochastic average in principle implies an average over an initinite number of realizations. The process $\{K_n\}$ is called ergodic, if the infinite space limit of the arithmetic average and its ensemble average coincide,

$$\lim_{w\to\infty} \frac{d}{w} \sum_{n=1}^{w/d} K_n = \overline{K}_A. \tag{4.15}$$

This implies that the heterogeneity features present in a single medium realization are representative of the ensemble of aquifers. Thus, in an ergodic medium, the stochastic average conductivity may be used to predict the effective hydraulic conductivity to be used to describe flow on a large scale. Large scale in this particular example means, large compared to the characteristic size of a stratum. Here we are primarily interested in ergodic processes because we want to use the stochastic approach to make predictions on flow and transport in heterogeneous media.

In general, hydraulic conductivity and other physical and chemical medium characteristics are continuous functions of the spatial position, $K(\mathbf{x})$. A more detailed account on the stochastic modeling approach in hydrogeology can be found in the

textbook by Dagan (1989), Gelhar (1993) and Rubin (2003).

Two-Dimensional Isotropic Media We consider the exactly solvable case of flow in isotropic two-dimensional media presented in Matheron (1967). Hydraulic conductivity $K(\mathbf{x})$ is modeled as a stationary and ergodic random field with the property that $K(\mathbf{x})$ and $K(\mathbf{x})^{-1}$ obey the same statistics. This is the case if $K(\mathbf{x}) = \exp[Y(\mathbf{x})]$ is multi-lognormally distributed with istropic correlation properties, i.e., $Y(\mathbf{x}) = \ln[K(\mathbf{x})]$ is multi-normally distributed. Cleary, the distribution of $K(\mathbf{x})^{-1} = \exp[-Y(\mathbf{x})]$ is again lognormally distributed. The following derivation uses the duality argument of Keller (1964), see also the paper by Dean et al. (2007).

The Darcy velocity is assumed to the divergence-free, i.e., $\nabla \cdot \mathbf{q}(\mathbf{x}) = 0$. Therefore, it can be represented in terms of a streamfunction $\psi(\mathbf{x})$ as $\mathbf{q}(\mathbf{x}) = -\mathbf{e}_3 \times \nabla\psi'(\mathbf{x})$, where $\mathbf{e}_3$ denotes the unit vector perpendicular to the two-dimensional flow plain. Darcy's law (4.10) relates conductivity $h(\mathbf{x})$ and hydraulic conductivity $K(\mathbf{x})$ to the streamfunction $\psi(\mathbf{x})$ as $K(\mathbf{x})\nabla h(\mathbf{x}) = \mathbf{e}_3 \times \nabla\psi(\mathbf{x})$. A vectorial multiplication of this equation from the left with $\mathbf{e}_3$ gives a dual relation between the streamfunction $\psi(\mathbf{x})$ and the inverse hydraulic conductivity $K(\mathbf{x})$ with the hydraulic head, $K(\mathbf{x})^{-1}\nabla\psi(\mathbf{x}) = -\mathbf{e}_3 \times \nabla h(\mathbf{x})$. By defining now $K'(\mathbf{x}) = K_0^2/K(\mathbf{x})$, such that the distributions of $K'(\mathbf{x})$ and $K(\mathbf{x})$ are identical, and further, defining $\psi'(\mathbf{x}) = \psi(\mathbf{x})/K_0$, we can write the following dual system of equations for $\psi'(\mathbf{x})$ and $h(\mathbf{x})$,

$$K(\mathbf{x})\nabla h(\mathbf{x}) = -K_0\mathbf{e}_3 \times \nabla\psi'(\mathbf{x}), \qquad K'(\mathbf{x})\nabla\psi'(\mathbf{x}) = K_0\mathbf{e}_3 \times \nabla h(\mathbf{x}). \tag{4.16}$$

As $K(\mathbf{x})$ and $K'(\mathbf{x})$ are statistically identical, we obtain for both averages $\overline{K(x)\nabla h(\mathbf{x})} = K^e\nabla\overline{h}(\mathbf{x})$ and $\overline{K'(x)\nabla\psi(\mathbf{x})} = K^e\nabla\overline{\psi}(\mathbf{x})$, respectively. As such, we obtain by averaging (4.16) the relation $K^e\nabla\overline{h}(\mathbf{x}) = -K_0\mathbf{e}_3 \times \nabla\overline{\psi'}(\mathbf{x})$. Vectorial multiplication from the left by $\mathbf{e}_3$ gives $K_0\nabla\overline{\psi'}(\mathbf{x}) = K^e\mathbf{e}_3 \times \nabla\overline{h}(\mathbf{x})$. This relation is now compared to the average of the second equation in (4.16), $K^e\nabla\overline{\psi'}(\mathbf{x}) = K_0\mathbf{e}_3 \times \nabla\overline{h}(\mathbf{x})$. Thus, we obtain directly that $K^e = K_0$. For the multi-lognormal random conductiv-

ity field with isotropic correlation function, it is easy to verify that $K_0 = K_G$, the geometric mean conductivity, such that $K^e = K_G$.

Three-Dimensional Isotropic Media The problem of finding effective hydraulic conductivity in three-dimensional heterogeneous porous media has been pursued in a systematic way by using stochastic modeling. In the following, we want to briefly outline the basic idea following the method presented in the paper by Gutjahr et al. (1978).

As above, hydraulic conductivity here is represented by a stationary isotropic multi-lognormally distributed spatial random field. The basic methodology consists in seeking an approximation for the effective hydraulic conductivity K^e of first order in the variance σ_Y^2 of log-hydraulic conductivity $Y(\mathbf{x})$. To this end, $Y(\mathbf{x})$ is separated in its ensemble mean value $\overline{Y}$ and fluctuations $Y'(\mathbf{x}) = Y(\mathbf{x}) - \overline{Y}$ about it. Along the same lines, hydraulic head $h(\mathbf{x})$ is decomposed into its mean value $\overline{h}(\mathbf{x}) = \overline{h}(\mathbf{x})$ and fluctuations $h'(\mathbf{x}) = h(\mathbf{x}) - \overline{h}(\mathbf{x})$ about it. It is furthermore assumed that the average hydraulic gradient is constant $\nabla\overline{h}(\mathbf{x}) = G_H\mathbf{e}_1$ and aligned with the one-direction of the coordinate system as a consequence of constant head boundary conditions. Using this decomposition in (4.10) and discarding terms that are of order higher than 2 in the fluctuating quantities, we obtain for the average Darcy flow

$$\overline{\mathbf{q}}(\mathbf{x}) = -K_G G_H \mathbf{e}_1 - K_G \left[\frac{\sigma_Y^2}{2} + \overline{Y'(\mathbf{x})\nabla h'(\mathbf{x})} \right], \tag{4.17}$$

where we used the expansion $K(\mathbf{x}) = K_G\left[1 + Y'(\mathbf{x}) + Y'(\mathbf{x})^2/2 + \dots\right]$ and the fact that by definition $\overline{Y'(\mathbf{x})} = \overline{h'(\mathbf{x})} = 0$. Notice that the lowest order term in (4.17) is identical to the exact result for two-dimensional isotropic media derived in the precious section.

In order to evaluate (4.17) consistently in σ_Y^2, it remains to determine an expression for $h'(\mathbf{x})$ linear in $Y'(\mathbf{x})$. To this end, we consider the flow equation for $h(\mathbf{x})$ in steady state, which is obtained by taking the divergence of (4.10) as $\nabla^2 h(\mathbf{x}) + \nabla Y(\mathbf{x}) \cdot \nabla h(\mathbf{x}) =$

0. Using the decompositions of $h(\mathbf{x})$ and $Y(\mathbf{x})$ in mean and fluctuations in the steady state flow equation, we obtain for $h'(\mathbf{x})$ the following equation

$$\nabla^2 h'(\mathbf{x}) = -\frac{\partial Y'(\mathbf{x})}{\partial x_1} G_H, \tag{4.18}$$

where we disregard contributions that are quadratic in the fluctuations. This Poisson equation can be solved, for example by the method of Green's functions such that $h'(\mathbf{x}) = \int d\mathbf{x}' Y'(\mathbf{x}') g(\mathbf{x}-\mathbf{x}') G_H$, where an infinite flow domain is assumed. The Green's function satisfies $\nabla^2 g(\mathbf{x}-\mathbf{x}') = -\delta(\mathbf{x}-\mathbf{x}')$ and is given by $g(\mathbf{x}) = 1/(4\pi|\mathbf{x}|)$. Inserting the expression for $h'(\mathbf{x})$ into (4.17) and solving the remaining integrals gives

$$\overline{\mathbf{q}}(\mathbf{x}) = -K_G \left[1 + \sigma_Y^2 \left(\frac{1}{2} - \frac{1}{3}\right)\right] G_H. \tag{4.19}$$

such that the effective conductivity is identified to be $K^e = K_G \left[1 + \sigma_Y^2 \left(\frac{1}{2} - \frac{1}{3}\right)\right]$. Notice that we used the dimensionality of space only when specifiying the Green's function to solve (4.18). The same perturbation calculation holds also for $d = 1$ and $d = 2$ dimensions. The general perturbation expression for the effective hydraulic conductivity in d spatial dimensions is given by $K^e = K_G \left[1 + \sigma_Y^2 \left(\frac{1}{2} - \frac{1}{d}\right)\right]$.

Notice that the arithmetic average of $K(\mathbf{x})$ is given by $K_A = K_G \exp(\sigma_Y^2/2)$, the harmonic average by $K_H = K_G \exp(-\sigma_Y^2/2)$. In analogy, starting from the above perturbation approximation for K^e it was conjectured (Gelhar and Axness, 1983) that $K^e = K_G \exp[\sigma_Y^2 \left(\frac{1}{2} - \frac{1}{d}\right)]$, which in the case of $d = 1$ reduces to the exact result $K^e = K_H$ and for $d = 2$ to the exact result $K^e = K_G$. In general it is found (Matheron, 1967) that the effective conductivity is bounded between the harmonic and arithmetic mean conductivities, $\overline{K}_H \leq K^e \leq \overline{K}_A$.

Anisotropic Media Statistically anisotropic media are characterized by directional dependence of the correlation length of the fluctuations of hydraulic conductivity. Notice that for anisotropic media, as pointed out above, effective dispersion is actually a tensorial quantity. The stochastic perturbative methdology is identical to the one

reviewed in the previous paragraph, with the difference that here the covariance of the loghydraulic conductivity fluctuations is directionally depended. Using this methodology, Gelhar and Axness (1983) derived explicit expressions for the hydraulic conductivity tensor in $d = 3$ spatial dimensions. Specifically, for a mean flow aligned with the bedding, i.e., aligned with the direction of stratification of the aquifer, and isotropic correlation length $\lambda_1 = \lambda_2 = \lambda_h > \lambda_3$ in the horizontal direction, these authors find that the effective hydraulic conductivity tensor is diagonal with isotropic conductivity in the horizontal, $K^e_{11} = K^e_{22} = K_h$, and a different value $K^e_{33} = K_v \neq K_h$ in the vertical. For this case, the results obtained by Gelhar and Axness (1983) can be written as (Sanchez-Vila et al., 2006)

$$K_h = K_G \left(1 + \frac{\chi}{2}\sigma_Y^2\right), \qquad K_v = K_G \left[1 - \left(\frac{1}{2} - \chi\right)\sigma_Y^2\right], \tag{4.20}$$

where χ is defined by

$$\chi = \frac{\rho^2}{\rho^2 - 1}\left[1 - \frac{\arctan\left(\sqrt{\rho^2 - 1}\right)}{\sqrt{\rho^2 - 1}}\right], \qquad \rho = \frac{\lambda_h}{\lambda_v}. \tag{4.21}$$

These expressions reduce to the ones for three-dimensional isotropic media presented above in the limit $\rho \to 1$.

Comprehensive reviews of approaches to determine the effective hydraulic conductivity for anisoptropic bounded and infinite porous media as well as for non-stationary conductivity fields can be found in the papers by Renard and de Marsily (1997) and Sanchez-Vila et al. (2006).

Further Remarks It remains to remark that effective or equivalent single phase flow properties in heterogeneous porous media have been intensely studied over the past 50 years, and the brief account given above is all but complete.

In the literature (Wen and Gómez-Hernández, 1996; Sanchez-Vila et al., 2006) a distinction is made between effective and equivalent hydraulic conductivities. The term effective hydraulic conductivity is defined in an ensemble sense in the context

of a stochastic aquifer model. Thus it relates ensemble average flux to an average head gradient. The equivalent hydraulic conductivity is defined in a single aquifer by spatial averaging. It relates the spatially averaged Darcy flux with the spatially average hydraulic gradient. Thus, equivalent hydraulic conductivities are representative of a certain region of the medium or medium block. We touched on this issue when reviewing equivalent conductivites in stratified media, and their representation in a stochastic model. Equivalent and effective hydraulic conductivities in this sense may be equated if the underlying medium or region of the medium has ergodic properties.

The necessity to define equivalent hydraulic conductivities arises in the problem of the representation of point measurements of hydraulic conductivity in a coarse numerical grid, the size of which, however, may not fulfil the ergodicity conditions required to equal ensemble and spatial average. The coarse-grained medium representation characterized by spatially variable (from block to block) equivalent conductivity is considered a large scale aquifer equivalent. Specifically, this equivalent medium should be characterized by the same mean flow as the fine scale medium. This requirement poses some consistency conditions for the equivalent conductivity values. They cannot be considered an intrinisc property of the medium block, but depend on the conductivities of the surrounding blocks; equivalent conductivies are in general non-local quantities (Neuman and Orr, 1993). Wen and Gómez-Hernández (1996), Renard and de Marsily (1997) and Sanchez-Vila et al. (2006) provide comprehensive review of approaches, methods and techniques for the determination of equivalent hydraulic conductivies.

The heterogeneous nature of a natural medium leads on one hand to large scale flow properties that are different from the local scale ones, which are quantified in the context of this section by effective and equivalent hydraulic conductivities. These heterogeneities, on the other hand, induce uncertainty on these averages, due to the incomplete knowledge of the details of the particular medium under consideration. The representation of the heterogeneous porous medium as a realization of an ensemble of

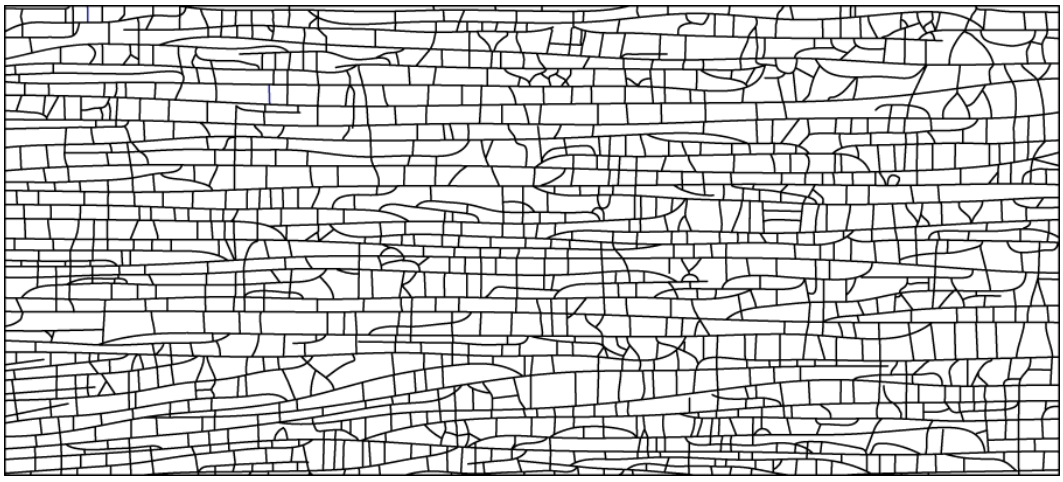

Figure 4.3: Sketch of a double continuum medium inspired by the geometry of the Bristol channel (Geiger et al., 2013).

media provides the framework for the quantification of uncertainty on hydraulic heads and equivalent conductivities (Dagan, 1986; Neuman and Orr, 1993). Winter et al. (2003) focus on the quantification of uncertainty in highly heterogeneous geological media that are composed of domains of very distint hydraulic properties. These authors consider heterogeneity in both the geometry of these domains as well as in the physical medium properties of each domain.

In the following section, we will briefly review the dual porosity approach for the modeling of flow in media with with sharp contrasts in hydraulic conductivity.

4.2.2.2 Unsteady Flow: Dual Continuum Media

In this section, we consider the situation that the local equilibrium condition invoked above is not valid, this means that hydraulic head is not in local equilibrium on the support scale of the spatially averaged model. Such conditions are typical for fractured media characterized by sharp contrasts between the hydraulic properties in the fracture and matrix domains.

Barenblatt et al. (1960) suggested a dual continuum model for flow in fractured media illustrated schematically in Figure 4.3. Both fracture and matrix domain are

represented by Darcy scale porous media characterized by distinct hydraulic condutivities, K_f and K_m, respectively, and specific storage coefficients, S_f and S_m, respectively. The volume fraction φ_f of the fracture domain is typicall much smaller than the volume fraction φ_m of the matrix domain, $\varphi_f \ll \varphi_m$. Notice that here the subscripts f and m refer to the fracture and matrix domains, respectively. The basis idea is to capture the large scale behavior by averaging the flow problem over a representative elementary volume of the medium but respect the disparity in the hydraulic properties in the two continua. Due to this disparity the heads in fracture and matrix may be very different.

Similar as for the upscaling from pore to Darcy scale, a REV here is defined as the averaging volume, for which the ratios of fracture to bulk volume and matrix to bulk volume converge to the characteristic constant values φ_f and φ_m. This requires that a characteristic matrix length scale exists. The REV represent the support volume of the large scale flow description, this means, the coordinate $\mathbf{x}$ in the large scale flow model represents a portion of the detailed medium description of the size of the REV.

Instead of defining a single average hydraulic head representative for the REV, the dual continuum approach defines intrinsic averages over the heads in the fracture and matrix domains as

$$h_f(\mathbf{x},t) = \frac{1}{V_f}\int\limits_{\Omega_f} d\mathbf{r} h(\mathbf{x}+\mathbf{r},t), \qquad h_m(\mathbf{x},t) = \frac{1}{V_m}\int\limits_{\Omega_m} d\mathbf{r} h(\mathbf{x}+\mathbf{r},t), \tag{4.22}$$

where Ω_f and Ω_m represent the fracture and matrix portions of the REV and V_f and V_m their respective volumina. The large scale flow behavior can then be described by the following coupled set of equations

$$S_f\varphi_f \frac{\partial h_f(\mathbf{x},t)}{\partial t} - K_f\varphi_f \nabla^2 h_f(\mathbf{x},t) = \Gamma(\mathbf{x},t), \tag{4.23}$$

$$S_m\varphi_m \frac{\partial h_m(\mathbf{x},t)}{\partial t} - K_m\varphi_m \nabla^2 h_m(\mathbf{x},t) = -\Gamma(\mathbf{x},t), \tag{4.24}$$

where the source term $\Gamma(\mathbf{x},t)$ quantifies mass transfer between the fracture and matrix continua. It can be determined by the requirement of head and flux continuum at the

interface between the fracture and matrix continua. The total hydraulic head $h_t(\mathbf{x}, t)$ in the REV is given by $h_t(\mathbf{x}, t) = \varphi_f h_f(\mathbf{x}, t) + \varphi_m h_m(\mathbf{x}, t)$.

The exchange term $\Gamma(\mathbf{x}, t)$ is estimated in Barenblatt et al. (1960) as

$$\Gamma(\mathbf{x}, t) = -\omega \left[h_f(\mathbf{x}, t) - h_m(\mathbf{x}, t) \right], \tag{4.25}$$

where the mass transfer rate ω is related to the matrix conductivity K_m and the characteristic block size dimensions. If the permeability in the matrix is significantly smaller than the permeability in the fracture, $K_m \ll K_f$, the direct contributions of the matrix to the macoscopic flow may be disregarded, i.e., $K_m = 0$ in (4.24). In this case the matrix continuum contributes to the large scale flow behavior in an indirect way and acts as a reservoir that exchanges mass with the fracture continuum. The exchange term $\Gamma(\mathbf{x}, t)$ can be then expressed in terms of the hydraulic head in the fracture continuum as

$$\Gamma(\mathbf{x}, t) = -\varphi_m S_m \frac{d}{dt} \int_0^t dt' g_m(t - t') h_f(\mathbf{x}, t') + \varphi_m S_m g_m(t) h_{m0}, \tag{4.26}$$

where the memory function $g_m(t) = \omega' \exp(-\omega' t)$ with $\omega' = \omega / (\varphi_m S_m)$, and h_{m0} is the initial head in the matrix. Notice that the specific form (4.25) assumes that the hydraulic head in the fracture is in quasi equilibrium. If this is not given, the memory function $g_m(t)$ is in general obtained by solving the flow problem in the fine scale matrix domain with fixed head $h_f(\mathbf{x}, t)$ at the fracture-matrix interface. Furthermore, if the matrix continuum is characterized by a distribution of characteristic matrix scales and matrix conductivies, this means, it is composed of a set of multiple continua, the source term $\Gamma(t)$ is given by the sum of the contributions of each of the different continua as $\Gamma(t) = \sum_i \varphi_{m,i} S_{m_i} g_{m,i}(t)$ with $\varphi_{m,i}$ and $S_{m,i}$ the volume fraction and specific storage of the ith matrix continuum, and $g_{m,i}(t)$ the memory function that quantifies the mass exchange between the fracture and ith matrix continuum.

4.3 Solute Transport

The following sections give a brief overview on transport upscaling from the pore to the field scale, and discusses large scale transport modeling approaches. Before this, we want to briefly discuss some of the assumptions that are related to continuum scale transport descriptions based on the well known advection-dispersion equation.

First, the concentration $c(\mathbf{x}, t)$ of a dissolved substance is defined over a support volume, or representative elementary volume $V_r \sim \ell^d$, over which concentration is assumed to be constant. The dimensionality of space is denoted by d, ℓ is a characteristic local scale. This means, it is assumed that a smallest support volume exists within which concentration gradients are essentially zero. Concentration can then be defined as

$$c(\mathbf{x}, t) = \frac{M(\mathbf{x}, t)}{V_r}, \tag{4.27}$$

where $M(\mathbf{x}, t)$ is the amount of solute contained in the volume V_r at the position $\mathbf{x}$ at time t. It is further assumed that concentration changes, or perturbations of the solute distribution over the support scale are accommodated, or relaxed on a time scale that is much smaller than the observation time scale T_{obs}. The physical relaxation mechanism on the local scale is diffusion or local dispersion. Thus, the characteristic relaxation time scale is given by $\tau_D = \ell^2/D$, with D a diffusion or dispersion coefficient. If the condition $\tau_D \ll T_{obs}$ is fulfilled, concentration changes in a given time interval Δt at a given position $\mathbf{x}$ only depend on the fluxes to and from the actual position within the time interval Δt. Under these conditions solute transport may be modeled by advective and dispersive mass transfer in terms of the advection-dispersion equation

$$\frac{\partial c(\mathbf{x}, t)}{\partial t} + \nabla \cdot \mathbf{u} c(\mathbf{x}, t) - D \nabla^2 c(\mathbf{x}, t) = 0, \tag{4.28}$$

where $\mathbf{u}$ is the transport velocity. Depending on the size of the support volume, or representative elementary volume, and the medium and flow properties, the above

conditions on uniqueness of concentration values on the local scale, and mass transfer properties, may not be fulfilled. In the following sections, we will discuss these issues and related scale effects on conservative transport from pore to Darcy and from Darcy to field scale.

4.3.1 Pore to Darcy Scale

Solute transport in the fluid portion Ω_f of a porous medium can be described by the advection-diffusion equation (Bear, 1972)

$$\frac{\partial C(\mathbf{x},t)}{\partial t} + \nabla \cdot [\mathbf{v}(\mathbf{x})C(\mathbf{x},t) - D\nabla C(\mathbf{x},t)] = 0 \tag{4.29}$$

where $C(\mathbf{x},t)$ is the solute concentration, $\mathbf{v}(\mathbf{x})$ is the Stokes velocity, and D is the effective molecular diffusion coefficient. The solid grains are assumed to be impermeable to both flow and transport. The transport problem (4.29) can also be formulated in am equivalent Lagrangian framwork in terms of the equation of motion of the position $\mathbf{x}(t)$ of solute particles. These are given by (Risken, 1996)

$$\frac{d\mathbf{x}(t)}{dt} = \mathbf{v}[\mathbf{x}(t)] + \sqrt{2D}\boldsymbol{\xi}(t), \tag{4.30}$$

where $\boldsymbol{\xi}(t)$ denotes a Gaussian white with zero mean and unit variance, which models the erratic motion of the solute particle due to diffusion.

The transport domain may be quite complex depending on the pore geometry, and as a consequence the flow field $\mathbf{v}(\mathbf{x})$ may be very variable. The complexity in the flow field as well as in the boundary conditions, make the pore scale flow and transport problem challenging, in terms of characterization and in terms of the actual solution of flow and transport due to the high number of degrees of freedom. For practical applications, however, it is desirable to have a transport description in terms of a few effective flow and transport parameters. As for the flow problem in the previous section, this requires averaging, or coarse graining of the pore-scale transport equation (4.29).

Taylor Dispersion We first consider the example of transport in a single pore that is idealized here for a two-dimensional medium by a channel with constant aperture $2a$. This example serves to illustrate a series of issues related to the upscaling of transport in heterogeneous media in general.

Due to the particular geometry, the flow velocity is aligned with the channel and depends only on the position along the channel cross-section. The solution of the flow equation (4.3) in steady state for a two-dimensional channel is given by the Hagen-Poiseuille profile

$$v(x_2) = v_0 \left[1 - \left(\frac{x_2}{a}\right)^2\right], \qquad v_0 = \frac{-a^2 \Delta p}{\mu L}, \tag{4.31}$$

where Δp is the pressure drop along the length L of the channel. The mean flow velocity over the channel cross-section is given by $v_m = 2v_0/3$. Transport in the channel is described by the advection dispersion equation

$$\frac{\partial C(\mathbf{x},t)}{\partial t} + v(x_2)\frac{\partial C(\mathbf{x},t)}{\partial x_1} - D\nabla^2 C(\mathbf{x},t) = 0. \tag{4.32}$$

This transport problem can be understood in terms of its characteristic length and time scales. The characteristic diffusion length over a time t is given by $\ell_D(t) = \sqrt{2Dt}$, while the characteristic advection length is given by $\ell_v = v_m t$. The characteristic scale $\tau_{vD} = 2D/v_m^2$ marks the time at which the two length scales are equal. The second characteristic time scale marks the time for complete diffusive mixing over the channel cross-section, $\tau_D = 2a^2/D$. For advection dominated transport, the two time scales are clearly separated, $\tau_{vD} \ll \tau_D$. The relative importance between adection and diffusion is measured by the Péclet number, which here is defined by $Pe = av_m/D = \sqrt{\tau_D/\tau_{vD}}$.

In the early time regime for $t \ll \tau_{vD}$, diffusive mass transfer is more efficient than advective, and therefore transport is essentially described by diffusion. In the late time regime for $t \gg \tau_D$ the solute is uniformly distributed over the channel cross-section and is essentially one-dimensional. In this late time regime, the solute distribution can

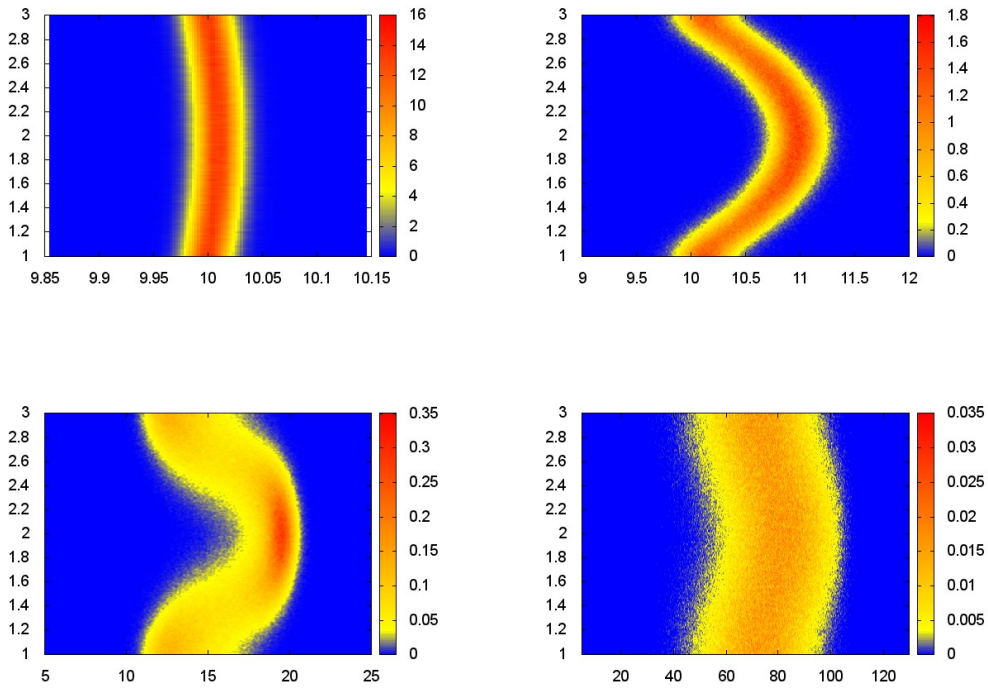

Figure 4.4: Solute plumes evolving from a line injection for $D = 10^2$, $u_0 = 1$ at times 10^{-2}, 1, 10 and 100.

be fully characterized in terms of the vertically averaged concentration

$$c(x_1, t) = \frac{1}{2a} \int_{-a}^{a} dx_2 C(\mathbf{x}, t). \tag{4.33}$$

For large Peclet numbers, the longitudinal solute dispersion is in general much larger than than given by molecular diffusion D. The non-uniform vertical velocity cross-section (4.31) leads to rapid solute transport in the center of the channel and slower transport at the channel boundaries. This leads to stretching of an initial line source as illustrated in Figure 4.4, and thus enhanced, purely advective solute spreading. This advective spreading induces vertical concentration gradients and thus vertical mass transfer, by which the solute eventually samples the vertical flow heterogeneity.

At times $t \gg \tau_D$, the solute has sampled the full velocity spectrum. In this regime an effective or equivalent dispersion coefficient can be defined in terms of the characteristic

spreading distance during the time τ_D. The characteristic spreading distance is given by $\delta v \tau_D$, where δv are the characteristic velocity fuctuations experienced by the solute. They are of the order of the mean velocity, $\delta v \sim v_m$. Thus, one obtains for the effective dispersion coefficient the estimate $D^e \sim v_m^2 \tau_D^2 / \tau_D = v_m^2 a^2 / D$, which reads for the non-dimensional dispersion coefficient as $D^e/D \sim Pe^2$. The exact value of the Taylor dispersion coefficient for channel flow is $D^e = \frac{2}{105} v_m^2 a^2 / D$, and for flow in a radial pipe, $D^e = \frac{1}{48} v_m^2 a^2 / D$, where here a is the pipe radius. The Taylor dispersion is inversely proportional to the molecular diffusion coefficients. The smaller molecular diffusion, the more time indvidual solute packets spend at different velocities, and thus, the larger the horizontal spread. Increasing diffusion reduces this contrast and therefore the Taylor dispersion coefficient. In the asymptotc time regime $t \gg \tau_D$, the evolution of the solute distribution is essentially one-dimensional and can be characterized by the advection-dispersion equation

$$\frac{\partial c(x_1,t)}{\partial t} + v_m \frac{\partial c(x_1,t)}{\partial x_1} - D^e \frac{\partial^2 c(x_1,t)}{\partial x_1^2} = 0. \tag{4.34}$$

Notice that the simplified representation of the advective terms, compared to (4.32) is compensated by an increased dispersion coefficient. The impact of velocity fluctuations on large scale solute transport is represented in terms of an effective dispersion coefficient. This concept is frequently used for large scale transport modeling in geophysical and turbulent fluid flows, as well as for the modeling of transport in heterogeneous porous media, as we will see in the following.

Before, that, let us consider briefly the dispersion behavior in the intermediate time regime $\tau_{vD} \ll t \ll \tau_D$. In this time regime, the solute is not in vertical equilibrium, this means concentration cannot be characterized by a single average value $c(x_1, t)$ at a longitudinal position x_1. Vertically averaged concentration profiles in this time regime are characterized by steep leading edge and a long trailing tail, see Figure 4.5. Such spatial features of a large scale solute plume, are often termed anomalous because they do not adjust themselves to advection-dispersion models such as the asymptotic equa-

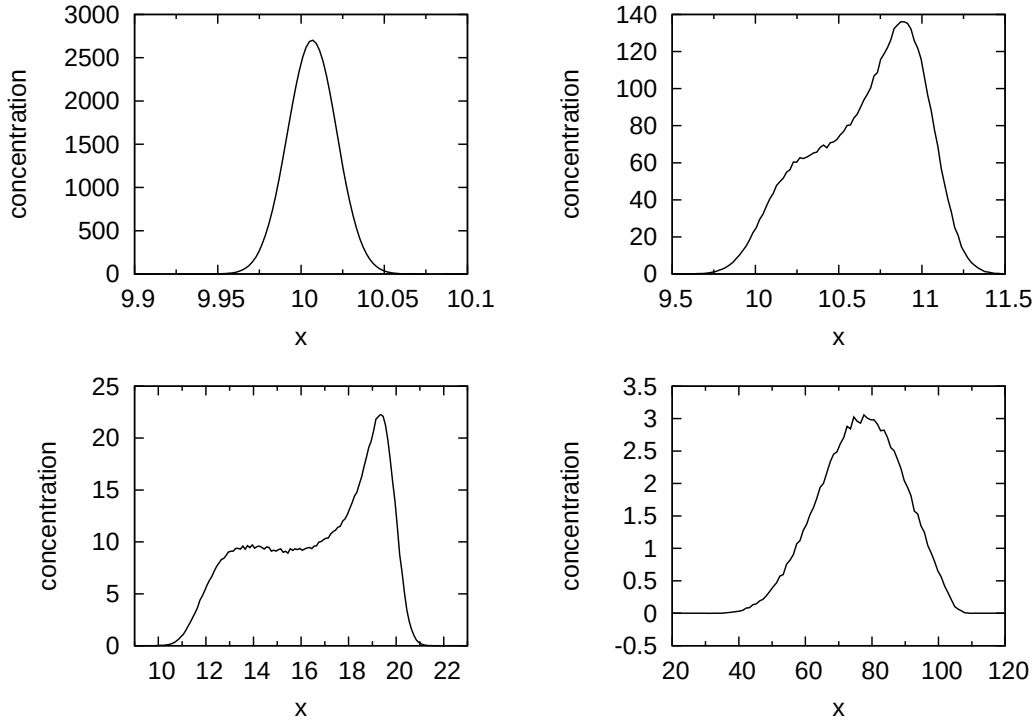

Figure 4.5: Vertically integrated solute concentration at times 10^{-2}, 1, 10 and 100.

tion (4.34). This behavior is also reflected in the behavior of the apparent longitudinal dispersion coefficient, which is defined as half the rate of change of the longitudinal second centered moment of the $C(\mathbf{x}, t)$ as (Aris, 1956)

$$D^a(t) = \frac{1}{2}\frac{d}{dt}\left\{\int_{-\infty}^{\infty} dx_1 \int_{-a}^{a} dx_2 x_1^2 C(\mathbf{x}, t) - \left[\int_{-\infty}^{\infty} dx_1 \int_{-a}^{a} dx_2 x_1 C(\mathbf{x}, t)\right]^2\right\}. \qquad (4.35)$$

In the asymptotic regime for $t \gg \tau_D$, it converges toward the constant D^e, while in the intermediate regimes it evolves from the local diffusion coefficient towards the asymptotic Taylor dispersion coefficient, see Figure 4.6. Such features, evolution of apparent dispersion, tails and leading edges in solute distributions, are the result of incomplete mixing on the support scale of the upscaled model, which here is the channel cross-section. Similar features are found in heterogeneous porous media on larger scales, as discussed in the introductory section and below. Another point can be made here. The basic mechanisms leading to anomalous behaviors, namely spatial and/or temporal

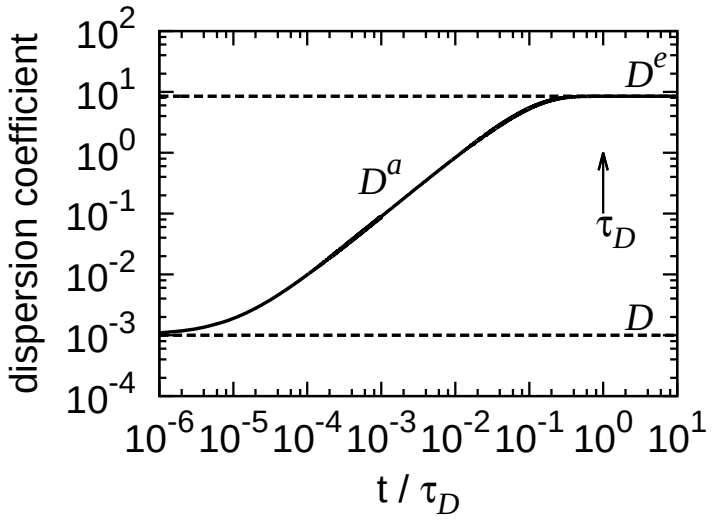

Figure 4.6: Temporal behavior of the apparent dispersion coefficent for $D = 10^{-3}$.

fluctuations, are the same mechamisms that ultimateley lead to scale effects in effective transport coefficients, if they exist.

Hydrodynamic Dispersion In the previous section, we considered transport in a single pore. For a porous medium, which can be seen as a network of pores, the dispersion behavior is generally different. Here the characteristic length scale is given by the typical pore length ℓ_p. Together with the average flow velocity v_m and diffusion, we can define the Péclet number $Pe = v_m \ell_p / D$, which compares the advection time scale $\tau_v = \ell_p / v_m$ and the diffusion time $\tau_D = \ell_p^2 / D$ over a pore length. Notice that the pore length marks the correlation scale for the fluctuations of the pore velocity $\mathbf{v}(\mathbf{x})$. Thus, we can obtain a rough estimate for the effect of pore-scale velocity fluctuations on the dispersion behavior of a solute. For large Peclet numbers, this means for advection dominated transport, the typical spread of the solute distribution after a few pore length will be given by square distance traveled during the advection time, $(v_m \tau_v)^2$ per advection time τ_v, which gives $D^e \sim v_m \ell_p$, and accordinlgy for the dimensionless dispersion coefficient $D^e / D \sim Pe$. Notice the difference between the scaling here and

the scaling of the Taylor dispersion coefficient above with Pe^2.

In general, it is found in experiments and pore-scale flow and transport simulations (Pfannkuch, 1963; Sahimi, 1995; Bijeljic and Blunt, 2006) that the longitudinal hydrodynamic dispersion coefficient depends non-linearly on the Péclet number. For $Pe < 1$, this means for diffusion dominated scenarios, $D^e/D \leq 1$ because diffusion is restricted by the solid matrix. For increasing $Pe > 1$, the longitudinal hydrodynamic dispersion coefficient evolves as $D^e/D \sim Pe^{1.2}$. Then for $Pe > 400$, this means in advection dominated scenarios, is behaves as $D^e/D \sim Pe$, as motivated above.

More rigorous treatments on the determination of hydrodynamic dispersion coefficients and the upscaling of transport from the pore to the Darcy scale use volume averaging (e.g., Whitaker, 1999) and homogenization theory (e.g., Hornung, 1997), moment methods (e.g., Brenner, 1980), as well as numerical porescale models (e.g., Meakin and Tartakovsky, 2009).

Upscaling the pore-scale transport problem (4.29) implies deriving the evolution equation for the volume averaged concentration

$$c(\mathbf{x}, t) = \frac{1}{V_f} \int\limits_{\Omega_f} d\mathbf{r} C(\mathbf{x} + \mathbf{r}, t), \tag{4.36}$$

Where V_f denotes the fluid volume within the representative elementary volume V_r. Volume averaging and homogenization theory derive and advection dispersion equation for Darcy scale transport that is given by (Bear, 1972)

$$\phi \frac{\partial c(\mathbf{x}, t)}{\partial t} + \nabla \cdot [\mathbf{q} c(\mathbf{x}, t) - \mathbf{D} \nabla c(\mathbf{x}, t)] = 0, \tag{4.37}$$

where ϕ is porosity, $\mathbf{q}$ is the Darcy velocity given by (4.10), and $\mathbf{D}$ is the hydrodynamic dispersion tensor.

Further Remarks It needs to be noticed that approaches that employ hydrodynamic dispersion coefficients assume that the support volume, the REV V_r, of the average, Darcy scale transport description is well mixed. This means that the solute

concentration can be uniquely defined at each position $\mathbf{x}$ in the coarse grained medium by it local average value. The dominant mechanism for concentration homogenization on the support scale is diffusion. This means that the times for which Equation (4.37) is valid need to be much larger than the diffusion time scale τ_D (Brenner, 1980), or in general the homogenization time scale over the support volume. This condition may not be met in media that are characterized by dead end pores and permeable solid grains that are accessible for solute diffusion. In such scenarios, the homogenization time scale may be much larger than the one estimated for diffusion in the pore space. Even though the medium properties such as porosity may be homogeneous on the REV scale, REV scale transport may deviate from the behavior predicted by the advection dispersion equation (4.37). These transport situation can be accounted for by multi-continuum approaches such as the ones proposed in Quintard and Whitaker (1994) and Lichtner and Kang (2007).

4.3.2 Darcy to Field Scale

As discussed in Section 4.2.2, Darcy scale heterogeneity in the physical medium properties induce spatial variability porosity and hydraulic conductivity. The latter induces spatial variability in the Darcy flow velocity through (4.10), and therefore also in the velocity depend hydrodynamic dispersion tensor. In addition, temporal fluctuation in the flow conditions may induce time dependence in the Darcy velocity and hydrodynamic dispersion. Thus, solute transport in a Darcy scale heterogeneous porous medium is expressed by the advection-dispersion equation

$$\phi(\mathbf{x})\frac{\partial c(\mathbf{x},t)}{\partial t} + \nabla \cdot [\mathbf{q}(\mathbf{x},t)c_i(\mathbf{x},t) - \mathbf{D}(\mathbf{x},t)\nabla c_i(\mathbf{x},t)] = 0 \tag{4.38}$$

As for porescale transport (4.29), also the Darcy scale transport problem (4.38) can be formulated in terms of the Lagrangian trajectories $\mathbf{x}(t)$ of "solute particles" (e.g., Dagan, 1989; Risken, 1996). The equation of motion for Darcy-scale solute particles is given by the Langevin equation (e.g., Kinzelbach, 1987; LaBolle et al., 1996; Salamon

et al., 2006; Delay et al., 2005),

$$\frac{\mathrm{d}\mathbf{x}_i(t)}{\mathrm{d}t} = \frac{\mathbf{q}[\mathbf{x}_i(t),t] - \nabla\cdot\mathbf{D}[\mathbf{x}_i(t),t]}{\phi[\mathbf{x}_i(t)]} + \sqrt{\frac{2\mathbf{D}[\mathbf{x}_i(t),t]}{\phi[\mathbf{x}_i(t)]}}\cdot\boldsymbol{\xi}(t), \tag{4.39}$$

where $\boldsymbol{\xi}(t)$ now is a Gaussian white noise characterized by zero mean and correlation $\xi_i(t)\xi_j(t') = \delta_{ij}\delta(t-t')$. It needs to be emphasized that the support scale of this description is the same as the one for (4.38). That is, the fact that here transport is represented in terms of solute particles does not imply that this description resolves spatial scales that are smaller than the support scale of the continuum description.

The continuum-scale physical medium properties as quantified by the hydraulic conductivity may in general vary on many scales. This spatial variability leads to large-scale transport behavior that is quantitatively different from its local scale counterpart. A manifestation of this scale behavior is the increase of solute dispersion with increasing scale (e.g., Lallemand-Barres and Peaudecerf, 1978; Gelhar et al., 1992) as quantified by macrodispersion coefficients (e.g., Gelhar and Axness, 1983; Dagan, 1984; Neuman et al., 1987). Other manifestations of spatial heterogeneity are so-called non-Fickian or "anomalous" transport features such as the tailing of breakthrough curves towards long times, and spatial solute distributions characterized by forward or backward tails, and the non-linear evolution of the spatial variance of the concentration distribution with time (Berkowitz et al., 2006; Neuman and Tartakovsky, 2008; Dentz et al., 2011b).

One may argue that the detailed knowledge of the spatial variability of the physical medium properties and the (numerical) solution of the local scale flow and transport problems (4.10) and (4.38), allows to quantify observed large scale transport behaviors. However, the detailed characterization of the local scale medium fluctuations is in many practical applications not possible and numerical transport simulators need to operate on coarse support scales due to limitations of computer power. But more than this, the observed "anomalous" large scale transport behaviors can be seen as collective phenomena that result from the interplay of medium heterogeneity on one hand and local scale flow and transport processes on the other. Thus, from a practical point of

view, it is essential to have coarse grained, average models at hand to quantify, explain and predict observed large scale transport phenomena. Methodologies to quantify spatial heterogeneity and its impact on transport include stochastic averaging (e.g., Gelhar and Axness, 1983; Dagan, 1984; Neuman et al., 1987; Rubin, 2003), volume averaging (e.g., Whitaker, 1999), homogenization theory (e.g., Hornung, 1997).

The macrodispersion approach (e.g., Gelhar and Axness, 1983) models effective transport by the same dynamical model as local scale transport. In this modeling framework, the evolution of the (ensemble) mean concentration $\overline{c}(\mathbf{x}, t)$ is given by

$$\overline{\phi}\frac{\partial \overline{c}(\mathbf{x}, t)}{\partial t} + \overline{\mathbf{q}} \cdot \nabla \overline{c}(\mathbf{x}, t) - \nabla \cdot \mathbf{D}^m \nabla \overline{c}(\mathbf{x}, t) = 0, \tag{4.40}$$

with $\overline{\phi}$ average porosity, $\overline{\mathbf{q}}$ the average Darcy velocity and $\mathbf{D}^m$ the macrodispersion tensor. Macrodispersion describes the action of flow heterogeneity on enhanced solute spreading, along the same lines as Taylor dispersion quantifies the impact of flow variability along a pipe cross-section, and hydrodynamic dispersion quantifies the effect of pore scale flow variability. In the context of transport in geophysical flows, the phenomenon of enhanced contaminant dispersion is described by eddy diffusivity.

Approaches to account for the impact of medium heterogeneity on the large scale transport behavior may be roughly divided into two groups. The first group quantifies the large scale behavior in terms of effective transport parameters such as macrodispersion coefficients, effective porosity and effective retardation coefficients, for example. It is often observed that effective transport parameters evolve with the time, or with travel distance of the transported solute. This gives an indication that the ADE based transport dynamics may be invalidated, along with the observation of non-Fickian large scale transport behaviors. As already mentioned at the end of the previous section, the validity of the advection-dispersion model (4.38) on the Darcy scale is conditional to the requirement of homogeneity of the REV, which may be invalidated depending on the spatial scales of the underlying heterogeneity and the mass transfer time scales. This is more so when passing from the Darcy to the field scale, where homogenization

scales may be much larger than the observation time scales.

Thus, the second groups seeks to cast the emerging non-Fickian transport dynamics in large scale equations and transport laws. Such models are often based on so-called non-local process models. This means that the change of concentration at a given time is influenced by the history of the transport process. This notion may be illustrated with the example of a double porosity medium characterized by a part that is mobile and one that is immobile with respect to advection. At a given point the average solute concentration is composed of a contribution from the mobile continuum that may pass fast and one of the immobile continuum that may have already been trapped for some time. Thus transport is determined by its history. This is also manifest in the double porosity flow model that defines two hydraulic heads at one point of the coarse grained flow domain.

4.3.2.1 Effective Transport Models

Heterogeneity induced large scale transport dynamics have been quantified in a series of approaches. Starting with the macrodispersion approach that represents transport by the large scale ADE (4.40) over blockeffective macrodispersion approaches to spatially and temporally non-local transport models.

Block-Effective Macrodispersion The block-dispersion approach accounts for the fact that the macrodispersion concept is only of limited applicability for practically relevant time and length scales. Instead, the medium is coarse grained into regions of characteristic size λ_c. While macrodispersion coefficients integrate the full spectrum of variabiliy of the flow fluctuations on spreading, block-effective dispersion coefficients quantify the flow fluctuations on a scale that is smaller than the coarse grainging scale λ_c. The coarse graining scale λ_c may be seen as the size of the grid block in a numerical model. While λ_c-scale fluctuations are accounted for explicitely in the numerical model, sub-scale fluctuations are quantified by block-effective macrodispersion coeffi-

cients (Beckie et al., 1996; Rubin et al., 1999). As the coarse graining scale increases, flow variability is transferred from advection to block-effective macrodispersion. The coarse graining scale may also been seen as the homogenization length scale of the physical model, or in other words as averaging scale at which concentration can be represented by a single average value.

Multirate Mass Transfer (MRMT) Approach The MRMT (Haggerty and Gorelick, 1995; Carrera et al., 1998) approach, or multicontinuum approach is based on the observation that non-Fickian transport in heterogeneous medium can be caused by the contrast of fast (advective) transport in regions of high flow velocity and slow transport in regions characterized by small flow velocities. This mechanism is modeled in the MRMT approach by dividing the medium into a mobile continuum, in which transport is due to advection and dispersion, and a set of immobile regions, in which transport can be due to diffusion and slow advection. The mobile and immobile regions are connected through linear mass transfer, which allows to quantify the medium heterogeneity in terms of the distribution of typical mass transfer times (e.g., Cunningham et al., 1997; Gouze et al., 2008; Willmann et al., 2008). This modeling framework is similiar in nature to the dual porosity approach for unsteady flow in fractured media. Notice that the behavior of the large scale concentration is given the average over the suite of local concentration values in the mobile and immobile continua. Thus, this approach represents the non-Fickian average transport behavior, and, explicitly, concentration variability at the support scale.

Continuous Time Random Walk (CTRW) Approach Similar as the MRMT approach, the CTRW framework (Berkowitz et al., 2006) is based on the observation that medium heterogeneity gives rise to a spectrum of characteristic mass transfer time scales. This means, that for a given characteristic transport distance, the mass transfer times scales vary due to the spatial heterogeneity of the medium. The CTRW approach

generalizes classical random walk (RW) models, such as (4.30) and (4.39). Classical RWs model solute transport in terms of random particle transitions in space during a constant time increment, that is, the particle trajectory is a stochastic process. CTRW generalizes this approach by introducing a distributed time increment that accounts for the variability of mass transfer time scales. This means, in a CTRW not only the spatial but also the time increment is modeled as a stochastic process. The impact of spatial heterogeneity is quantified by the joint distribution of transition length and times (e.g., Berkowitz and Scher, 1997; Le Borgne et al., 2008; Dentz and Castro, 2009). It has been shown that the MRMT and CTRW approaches are equivalent under some conditions (Dentz and Berkowitz, 2003).

Moment Equations and Projector Formalism Moment equations represent the governing equations for the statistical (ensemble) moments of the solute concentration such as the mean concentration and the mean squared concentration. This approach is based on a stochastic interpretation of the Darcy-scale ADE (4.38). This method yields spatio-temporally non-local equations for the mean concentration, concentration variance, and in principle also for the higher order ensemble concentration moments (e.g., Morales-Casique et al., 2006). The resulting moment equations are characterized by memory kernels which in principle can be related to the statistics of the underlying heterogeneity.

The projector formalism (e.g., Cushman and Ginn, 1993; Cushman et al., 2002) determines the ensemble moments of concentration by stochastic averaging of the concentration distribution in terms of the particle trajectories given by (4.39). Like the moment equation approach, the projector formalism yields effective equations for the ensemble concentration moments that are characterized by memory kernel that are related to the heterogeneity statistics.

Fractional Advection-Dispersion Equations Fractional-advection dispersion equations (e.g., Benson et al., 2000; Cushman and Ginn, 2000) generalize the ADE to the effect of introducing fractional-order space and time derivatives (West et al., 2003). Fractional-order space and time derivatives of a given function can be seen convolutions of this function with a power-law kernel function (in space or time). Time-fractional ADEs can be shown to be equivalent to CTRWs characterized by power-law transition time distributions (Metzler and Klafter, 2000) and MRMT (Schumer et al., 2003). Space-fractional ADEs may be related Levy flight random walk model, this means RWs characterized by a power-law distribution of space increments (Meerschaert et al., 2001; Metzler and Klafter, 2000). The phenomenological basis is again the realization that non-Fickian transport may be caused by broad distribution of mass transfer time scales.

Stochastic-Convective Streamtube Approach The stochastic streamtube approach models the heterogeneous medium as a set of individual streamtubes that are characterized by different, but typically constant flow velocities (e.g., Dagan and Bressler, 1979; Ginn et al., 1995; Cirpka and Kitanidis, 2000). Flow heterogeneity is accounted for statistically by the distribution of flow velocities across the different streamtubes. Transport in a single streamtube is given by the one-dimensional advection-dispersion equation characterized by constant transport parameters. The average concentration is then given by the sum of the partial concentration in the different stremtubes weighted by the distribution of streamtube velocities.

4.3.2.2 Mixing

In the previous section, we focused on models to describe average transport in heterogeneous media. We mentioned that non-Fickian transport can be caused by the notion of incomplete mixing, this means concentration variability on the support volume. In this section, we focus on mixing processes in heterogeneous media. Mixing is the process that leads to homogenization of heterogeneous concentration distributions,

dilution of concentrated solution, and is a precondition for chemical reactions as it puts segregated chemical species into contact.

In homogeneous media under uniform and constant flow conditions, solute mixing is due to local scale dispersion. For heterogeneous media this is different. The spatial heterogeneity of the field leads to stretching and folding of the solute plume. At times that are smaller than the mass transfer time over a typical heterogeneity scale, these mechanisms increase the solute spread but not the mixing of the solute (e.g., Kitanidis, 1994). Thus, for heterogeneous media, the processes of spreading and mixing need to be separated. Both processes are of course closely coupled. The concentration contrasts that are generated by the spread of the solute enhance mass transfer due to diffusion and local dispersion and thus lead to enhanced mixing. In the following we will briefly describe measures for these processes in terms of effective dispersion coefficients and concentration variability.

Effective Dispersion Coefficients Motivated by the fact that mixing in homogeneous media is fully quantified in terms of diffusion and dispersion, macroscale dispersion may be considered as a large scale mixing process. However, we have already seen, when discussing transport in a channel that the Taylor dispersion coefficient describes solute transport only at asymptotically large times, this means at times much larger than the diffusion time over the channel cross-section.

Macroscopic dispersion coefficients can be defined by the method of moments (e.g., Aris, 1956) in terms of the rate of growth of the variance of the average spatial solute distribution. Average here is understood to be a stochastic average. The ensemble variance is quantified by the second centered moment of the average concentration $\overline{c}(\mathbf{x}, t)$

$$\kappa_{ij}^{ens}(t) = \int \mathrm{d}\mathbf{x} x_i x_j \overline{c}(\mathbf{x}, t) - \int \mathrm{d}\mathbf{x} x_i \overline{c}(\mathbf{x}, t) \int \mathrm{d}\mathbf{x} x_j \overline{c}(\mathbf{x}, t), \tag{4.41}$$

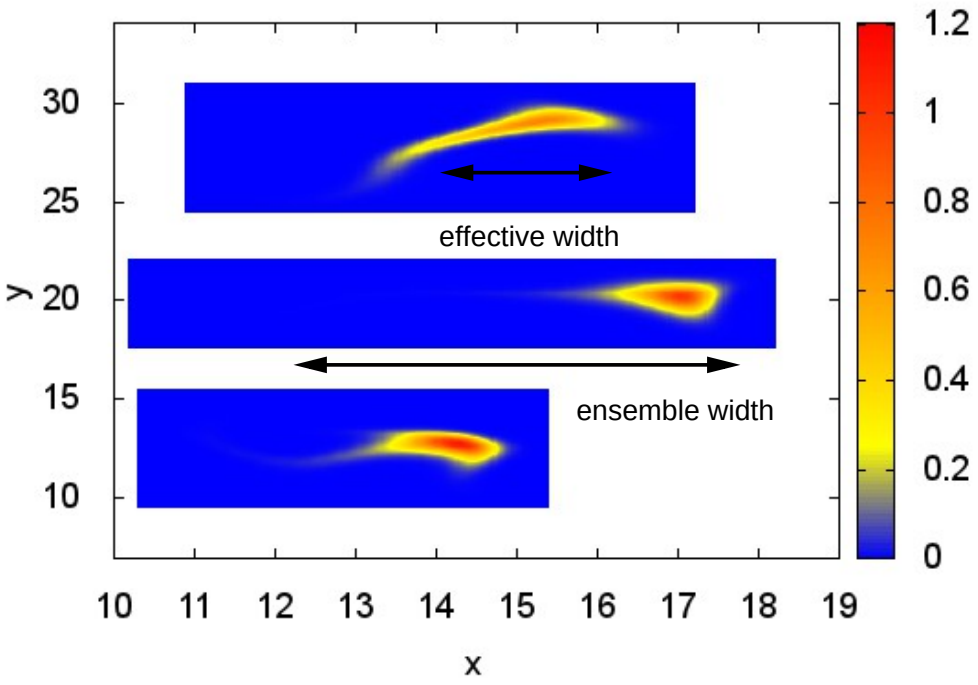

Figure 4.7: Illustration of the difference between the ensemble and effective measures for the plume width. The figures shows three plumes evolving from point-injections along the line at $x_1 = 10$ at time $t = 5\tau_q$ in 3 different realizations of a heterogeneous flow field.

and its temporal change is defined as the ensemble dispersion coefficients

$$D_{ij}^{ens}(t) = \frac{1}{2}\frac{d\kappa_{ij}^{ens}(t)}{dt}. \tag{4.42}$$

The macrodispersion coefficients in (4.40) are given by the long time limits $D_{ij}^{m} = \lim_{t\to\infty} D_{ij}^{ens}(t)$ if they exist. For transport in stratified media with infinite transverse extension, this is not the case (e.g., Matheron and de Marsily, 1980) for example.

Using stochastic modeling, Gelhar and Axness (1983) obtained for the longitudinal macrodispersion coefficient in the limit of large Péclet numbers

$$D_L^m = \sigma_Y^2 \overline{q} \lambda, \tag{4.43}$$

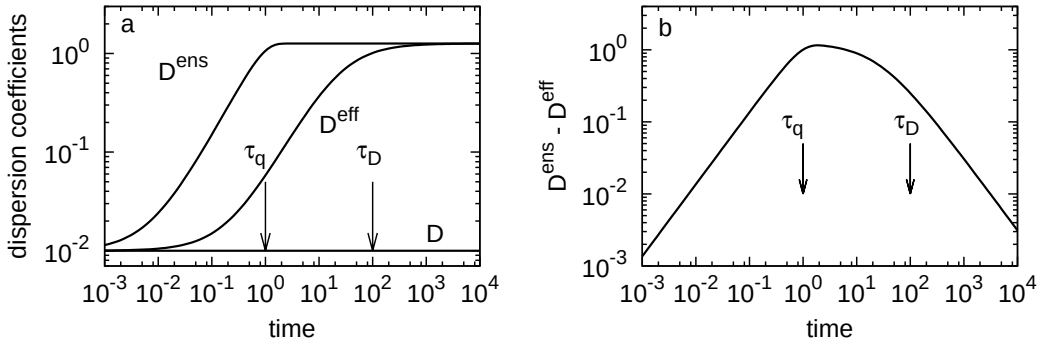

Figure 4.8: Illustration of (a) longitudinal effective versus ensemble dispersion coefficients and (b) growth rate of center of mass fluctuations.

where σ_Y^2 is the variance of the log-hydraulic conductivity field and λ its correlation length and $\overline{q}$ the average flow velocity. This result was obtained using a first-order perturbation expansion in σ_Y^2. In this approximation, the transverse dispersion coefficient turns out to be of the order of the local dispersion coefficient. Notice that the basic dependence on correlation length and mean velocity is the same as the one obtained for hydrodynamic dispersion above because the underlying physical processes are the same.

The ensemble dispersion coefficients (4.42) evolve in time (Dagan, 1988) on the advection time scale $\tau_q = \lambda/\overline{q}$. Ensemble dispersion measures the spreading of the average plume. As illustrated in 4.7, in addition to the spreading of the individual plumes, it quantifies an artificial spreading effect due to variability in the center of mass positions between different plume realizations.

The spatial variance of the solute distribution in a single realization is given by

$$\kappa_{ij}(t) = \int \mathrm{d}\mathbf{x} x_i x_j c(\mathbf{x},t) - \int \mathrm{d}\mathbf{x} \int \mathrm{d}\mathbf{x}' x_i x_j' c(\mathbf{x},t) c(\mathbf{x}',t). \tag{4.44}$$

The effective spatial variance of the concentration distribution is defined by the ensemble average over the variance in each realization, $\kappa_{ij}^{eff}(t) = \overline{\kappa_{ij}(t)}$, as illustrated in 4.7. The difference between the ensemble and effective variances is exactly the center of mass fluctuations between realizations (Batchelor, 1949, 1952; Kitanidis, 1988). Thus,

the effective dispersion coefficient, defined as half the temporal rate of change of the effective width

$$D_{ij}^{eff}(t) = \frac{1}{2}\frac{d\kappa^{eff}(t)}{dt} \tag{4.45}$$

measures the average spreading behavior in a single aquifer realization.

The evolutions of the longitudinal ensemble and effective dispersion coefficients for a solute plume that evolves from a point injection can be approximated for $Pe \gg 1$ and $\sigma_Y^2 < 1$ by (Dentz et al., 2000)

$$D_{11}^{ens} = \sqrt{\frac{\pi}{2}}\sigma_Y^2 \overline{q}\lambda \mathrm{erf}(t/\tau_q), \qquad D_{11}^{eff} = \sqrt{\frac{\pi}{2}}\sigma_Y^2 \overline{q}\lambda \left[1 - (1 + 4t/\tau_D)^{-\frac{d-1}{2}}\right]. \tag{4.46}$$

Their temporal evolution is illustrated in Figure 4.8. The effective dispersion coefficients evolve on the dispersion time scale $\tau_D = \lambda^2/D$, which measures the time for dispersive mass transfer over a correlation length of the medium. This reflects the physical mechanisms that eventually lead to macroscopic dispersion for a point source. At early times, smaller than τ_q, the solute has not experienced flow heterogeneity because the plume has not yet traveled over a correlation distance of the flow field. For times larger than τ_q, the plume is exposed to flow heterogeneity. It starts to be deformed by the flow field, and concentration gradients are created due to the stretching and compression of the material elements the solute plume is composed of. This is illustrated in Figure 4.9. This figure illustrates also that the effective variance κ_{11}^{eff} measures, at intermediate times $\tau_q < t < \tau_D$, the rate by which the plume spreads due to advective heterogeneity rather than actual mixing. However, an equivalent Gaussian plume characterized by the effective dispersion coefficient overestimates the actual solute dilution because it overestimates the actual volume occupied by the solute. In the following, we will discuss measures to describe the process of mixing and and the dilution state of a system.

Mixing and Dilution The dilution index was introduced by Kitanidis (1994) in order to describe the actual dilution state of a transport system. It is based on the

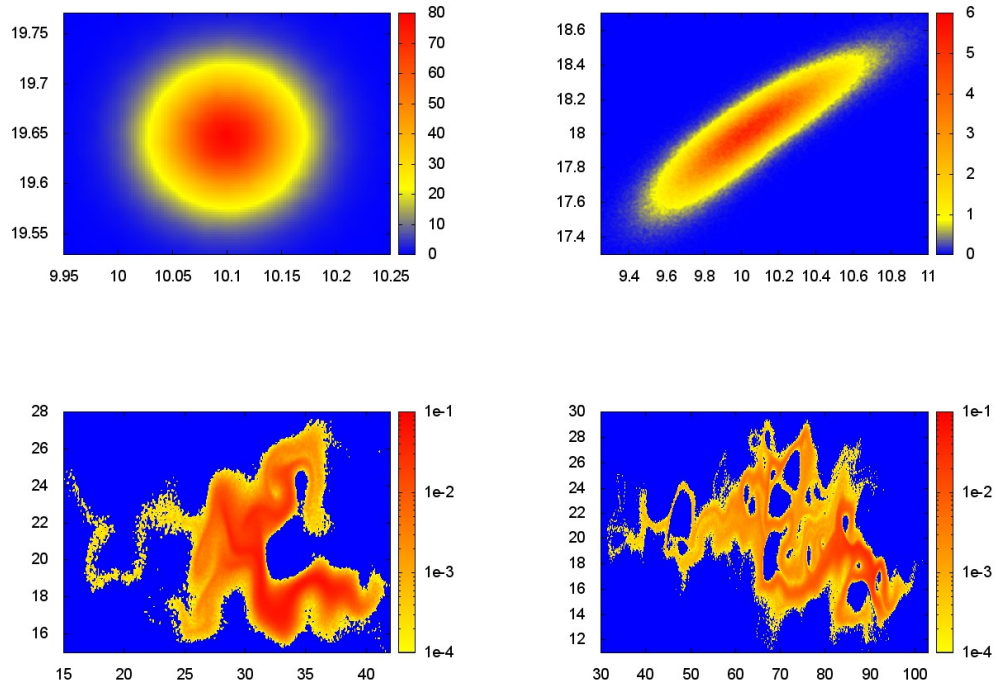

Figure 4.9: Solute plumes evolving from a point injection in a heterogeneous flow field for $Pe = 10^2$ at times $10^{-1}\tau_q$, τ_q, $20\tau_q$ and $50\tau_q$.

entropy of the normalized concentration distribution $c(\mathbf{x}, t)$, which is defined by

$$H(t) = -\int d\mathbf{x} c(\mathbf{x}, t) \ln[c(\mathbf{x}, t)]. \tag{4.47}$$

$H(t)$ is a measure for the amount of space the solute may occupy, or more precisely, it quantifies the logarithm of the volume accessed by the solute. Thus, the exponential of the entropy $H(t)$,

$$E(t) = \exp\left[H(t)\right]. \tag{4.48}$$

is a measure for the volume occupied by solute. $E(t)$ is called the dilution index. Kitanidis (1994) shows that the temporal change of the system entropy for a $c(\mathbf{x}, t)$ that satisfies (4.38) is given by

$$\frac{dH(t)}{dt} = \frac{1}{\phi} \int \frac{d\mathbf{x}}{c(\mathbf{x}, t)} \left[\nabla c(\mathbf{x}, t) \mathbf{D} \nabla c(\mathbf{x}, t)\right]. \tag{4.49}$$

In the absence of dispersion and diffusion, that is, in the absence of local scale mixing mechanisms, the entropy is given by the one of the initial system, $H(t) = H_0$ and the dilution index accordingly, $E(t) = E_0$. This means in the absence of dispersion, the entropy of the system remains constant. This is evident because the flow fields under consideration are volume conserving because of $\nabla \cdot \mathbf{q}(\mathbf{x}) = 0$. Notice also that entropy $H(t)$ in an infinite domain is maximized by a Gaussian distribution.

The expression in the square brackets in (4.49) represents the mechanism leading to dilution, namely the attenuation of concentration gradients by local dispersion. This is expression is closely related to what is known in the turbulence community as the scalar dissipation. The scalar dissipation rate describes the velocity by which concentration variability is destroyed. Concentration variability is measured in terms of the evolution of the global concentration variance σ_c^2

$$\sigma_c^2(t) = \int d^d x \overline{c'(\mathbf{x}, t)^2}, \tag{4.50}$$

where the concentration fluctuations are $c'(\mathbf{x}, t) = c(\mathbf{x}, t) - \overline{c}(\mathbf{x}, t)$. Based on (4.38), one obtains an evolution equation for the concentration variance (Kapoor and Kitanidis,

1998)

$$\frac{d\sigma_c^2(t)}{\mathrm{d}t} = -\frac{2}{\phi}\int \mathrm{d}^d x \left[\overline{\nabla c'(\mathbf{x},t)\mathbf{D}\nabla c'(\mathbf{x},t)} - \nabla\overline{c}(\mathbf{x},t)\mathbf{D}^m\nabla\overline{c}(\mathbf{x},t)\right], \tag{4.51}$$

This relation can be seen as a balance equation for concentration variability. The second term on the right hand side is quantified terms of the macrodispersion tensor and the average concentration. It is a source terms and represents the creation of concentration variance due to spreading. The first term is the scalar dissipation rate. It is a sink terms that represents the desctruction of concentration variability due local scale dispersion.

Notice that (4.51) is not closed because it depends on the local concentration fluctuations. The interaction by exchange with the mean (IEM) model (Villermaux and Devillon, 1972) approximates the scalar dissipation rate by an expression linear in σ_c^2 so that the first term on the right of (4.51) describes first order degradation. Other closure approximation employed in the turbulence literature can be found in Pope (2000). It turns out that the simple IEM closure cannot describe the decay of concentration variance in porous media (De Dreuzy et al., 2012).

We discussed above that the notions of incomplete mixing and non-Fickian transport are closely related. Non-Fickian transport can be seen as a consequence of the fact that the macroscopic support volume is not well mixed. Le Borgne et al. (2011) investigated the evolution of the scale at which concentration variability is negligible. Intuitively one would assume this mixing scale evolves diffusively according to $\sqrt{Dt}$, which is the case in a homogeneous medium. For strongly heterogeneous media, however, the action of the heterogeneous flow field distorts the plume and counteracts the homogenization by local dispersion. As a consequence of this competition, the mixing scale evolves slower than in a homogeneous medium, which indicates persistent non-Fickian transport in heterogeneous media.

Most effective models summarized above describe transport in terms of the average concentrations. As we have seen here, the mixing process is related to the creation

and attenuation of local scale concentration gradients, this means, it is a local process. Thus, the correct quantitifation of mixing in a large scale transport model requires a measure for local scale concentration variability. This relates to another issue intrinsic to spatial heterogeneity, namely uncertainty. Incomplete knowledge on the fluctuation details of the heterogeneous medium induce uncertainty on the concentration values. Incomplete mixing and uncertainty can be quantified in terms of the probability density function (PDF), $p_c(c, \mathbf{x}, t)$ of concentration at a given spatial position of the coarse grained medium (Pope, 2000; Lichtner and Tartakovsky, 2003). The distribution of concentration PDFs may be determined using Monte-Carlo simulations in a stochastic framework or by local spatial sampling of concentration values. (Semi)-analytical approaches are based on PDF equations, this means evolution equations for $p_c(c, \mathbf{x}, t)$, or so-called mapping approaches.

The knowledge of the local concentration variability and a correct representation of mixing are of particular importance for the modeling of reactive transport in heterogeneous media because chemical reactions are intrinsically local phenomena that rely on mass transfer to bring the chemical species into contact.

4.4 Reactive Transport

Reactive transport is in general modeled by the combination of a conseravtive transport equation that accounts for the evolution of the concentration due to physical mass transfer mechanisms and a source term, the reaction rate, which accounts for chemical reactions. In the previous section, we discussed conservative transport models at pore, Darcy and field scales. We emphasized that homogeneity of concentration at the relevant support scale plays an important role, which can be related to characteristic mass transfer time scales over the support volume. In the context of reactive transport, additional characteristic times emerge, the characteristic reaction scales τ_r.

Chemical reaction rate laws are typically determined in well mixed environments.

This means there are no mass transfer limitations, or, in other words, concentration changes due to physical mass transfer are equilibrated on time scales much smaller than the times scales τ_r for changes in the species concentrations due to chemical reactions. The relation of the characteristic physical mass transfer time scales τ_m on the support scale and the reaction time scale τ_r is measured by the Damköhler number

$$Da_{mic} = \frac{\tau_m}{\tau_r}. \tag{4.52}$$

Thus, for a microscopic Damköhler number $Da_{mic} \ll 1$, the evolution of the concentration of a given species i can be described by the rate law

$$\frac{dc_i(t)}{dt} = r[\{c_j(t)\}], \tag{4.53}$$

with $r[\{c_j(t)\}]$ the reaction rate that in general depends on the concentrations of all reacting species. As mentioned above, the formulation (4.53) requires that the support volume on which the species concentration $c_i(t)$ is defined is well mixed at any time. This implies that concentration can be defined locally by a single value, and that concentration changes on the support scale occur on time scales smaller than the reaction time scales. Under these conditions, reactive transport can be described by the advection-dispersion reaction equation (ADRE)

$$\frac{\partial c_i(\mathbf{x},t)}{\partial t} + \nabla \cdot \mathbf{u} c_i(\mathbf{x},t) - D\nabla^2 c_i(\mathbf{x},t) = r[\{c_j(\mathbf{x},t)\}. \tag{4.54}$$

As we have seen in the previous section, for transport in heterogeneous media, uniqueness of concentration on the support scale is not always given, again depending on the medium heterogeneity and the associated mass transfer time scales. In the following, we discuss these issues in relation to reactive transport modeling from the pore to the Darcy and Darcy to the field scale.

4.4.1 Pore to Darcy Scale

At the pore scale, the evolution of the concetration $C_i(\mathbf{x},t)$ of an aqueous species i can be expressed by a combination of the ADE (4.29) and suitably chosen source terms

and boundary conditions,

$$\frac{\partial C_i(\mathbf{x},t)}{\partial t} + \nabla \cdot [\mathbf{v}(\mathbf{x})C_i(\mathbf{x},t) - D\nabla C_i(\mathbf{x},t)] = \sum_j \nu_{ij} r_j[\{C_n(\mathbf{x},t)\}]. \tag{4.55}$$

We assume that the molecular diffusion coefficient D is the same for all species. The notation $\{C_n(\mathbf{x},t)\}$ indicates the set of all species concentrations. The reaction rate for the jth homogeneous reaction is denoted by by $r_j[\{C_n(\mathbf{x},t)\}]$ with the ν_{ij} the stoichiometric coefficients. As outlined above this formulation assumes that mass transfer on the microscopic support scale can be disregarded. The reaction rate on the right side represents fast and slow chemical reactions in the fluid phase. The terms fast and slow now refer to the typical reaction time scales compared to the diffusion time scale τ_D over a characteristic medium length scale, which are compared by the Damköhler number Da_j

$$Da_j = \frac{\tau_D}{\tau_{r,j}} \tag{4.56}$$

with $\tau_{r,j}$ the reaction time scale of the j-th reaction. Notice that the Damköhler number defined here is different from Da_{mic} defined above, which refers to mass transfer on the microscopic support volume. Fast chemical reaction, this means reactions j for which $Da_j \gg 1$, react almost instantenously upon a concentration change due to physical mass transfer. Such reactions are intrinsically mixing-limited.

For fast reversible reactions, indexed in the following by f, the species concentrations are related by the mass action law (e.g., Steefel and MacQuarrie, 1996; Saaltink et al., 1998)

$$\prod_i [\gamma_i c_i(\mathbf{x},t)]^{\nu_{fi}} = K_f, \tag{4.57}$$

where K_f is the equilibrium constant of the fth equilibrium reaction. The γ_i are the activity coefficients of the ith species, which depend in general on all species concentrations. Here we assume them to be constant. The reaction rates for $r_f[\{C_n(\mathbf{x},t)\}]$

can in principle be approximated by their limit for $Da_f \to \infty$ (Sanchez-Vila. et al., 2007)

$$r_f^e(\mathbf{x},t) = \lim_{Da_f \to \infty} r_f[\{C_n(\mathbf{x},t)\}]. \tag{4.58}$$

where $r_f^e(\mathbf{x},t)$ is the equilibrium reaction rate of the fth reaction. It can be expressed in terms of the transport and mixing dynamics of the conservative transport system (De Simoni et al., 2005, 2007). The right side of (4.55) can now be written as

$$\sum_j \nu_{ij} r_j[\{C_n(\mathbf{x},t)\}] = \sum_f \nu_{if} r_f^e(\mathbf{x},t) + \sum_s \nu_{is} r_s[\{C_n(\mathbf{x},t)\}]. \tag{4.59}$$

where we indexed the slow reactions by s.

Reactions between the fluid and solid phases take place at the fluid-solid boundaries where minerals are present. We focus here on precipitation-dissolution reactions. The boundary conditions at the fluid solid interface can then be written as (e.g., Lichtner and Kang, 2007; Whitaker, 1999)

$$-\mathbf{n}_{fs}(\mathbf{x}) \cdot D\nabla C_i(\mathbf{x},t)|_{\mathbf{x}\in\partial\Omega_s} = -\sum_m \nu_{im}\alpha_m(\mathbf{x}) j_m[\{C_n(\mathbf{x},t)\}]|_{\mathbf{x}\in\partial\Omega_s}, \tag{4.60}$$

where $\mathbf{n}_{fs}(\mathbf{x})$ is the unit normal vector on $\partial\Omega_s$ pointing from the fluid into the solid phase; $\alpha_m(\mathbf{x})$ is the relative mineral surface area. The relative mineral surface area is non-zero only at those locations on the solid fluid interface where the mineral is present. The reaction flux of the mth mineral at its surface is denoted by $j_m[\{C_n(\mathbf{x},t)\}]$. It depends on the aqueous concentrations at the solid surface. A discussion of the boundary conditions at the fluid-solid interface can be found in (Knabner et al., 1995).

Based on transition state theory (Hänggi et al., 1990) the reaction flux $j_m[\{C_n(\mathbf{x},t)\}]$ at the solid-fluid boundary may be modeled as (e.g., Lichtner and Kang, 2007)

$$j_m[\{C_n(\mathbf{x},t)\}]|_{\mathbf{x}\in\Omega_s} = k_m\left(1-\Omega_m(\mathbf{x},t)\right), \tag{4.61}$$

where k_m is the kinetic rate constant. The saturation state $\Omega_m(\mathbf{x}, t)$ is given by

$$\Omega_m(\mathbf{x}, t) = K_m^{-1} \prod_j \left[\gamma_j C_j(\mathbf{x}, t)\right]^{\nu_{jm}}, \qquad \mathbf{x} \in \Omega_s. \tag{4.62}$$

K_m is the equilibrium constant of the mth mineral reaction, ν_{jm} are the stoichiometric coefficients and γ_j denotes the activity coefficient of the jth aqueous species. The activity coefficients relate the species activities to their molal concentration. For mineral species, it is equal to one.

For practical applications of reactive transport modeling on the Darcy and field scale, the full characterization of the physical and chemical pore scale medium properties and the (numerical) solution of the porescale reactive flow and transport problems on macrosopic length scale are virtually impossible. As for the problems of single phase flow and conservative transport, upscaled reactive transport models are required which depend only on a few effective flow, transport and reaction parameters. Reactive transport is affected by physical heterogeneity which affects solute mixing and thus conservative mass transfer time scales as well as chemical heterogeneity, for example in the specific reactive surface areas.

Mathematical approaches to reactive transport upscaling from the pore to the Darcy scale has used volume averaging (Edwards et al., 1993; Quintard and Whitaker, 1994; Kechagia et al., 2002; Lichtner and Kang, 2007), Homogenization theory (Mikelic et al., 2006), pore-network modeling (Meile and Tuncay, 2006; Li et al., 2006) and smoothed particle hydrodynamics (Tartakovsky et al., 2008; Battiato et al., 2009). Traditionally, Darcy scale transport is quantified by an ADRE characterized by effective transport and reaction parameters which can be obtained from volume averaging of the porescale reactive transport problem (4.55). The evolution equation for the volume averaged species concentration $c_i(\mathbf{x}, t)$ is then given by(Lichtner, 1985; Quintard and Whitaker,

1994)

$$\phi(\mathbf{x})\frac{\partial c_i(\mathbf{x},t)}{\partial t} + [1-\phi(\mathbf{x})]\frac{\partial s_i(\mathbf{x},t)}{\partial t} + \nabla\cdot[\mathbf{q}(\mathbf{x},t)c_i(\mathbf{x},t) - \mathbf{D}(\mathbf{x},t)\nabla c_i(\mathbf{x},t)] =$$
$$\phi(\mathbf{x})\sum_i \nu_{ij} r_j[\{c_n(\mathbf{x},t)\}] + r_i^{(s)}[\mathbf{x},\{c_n(\mathbf{x},t)\}], \tag{4.63}$$

The bulk reaction rate for the fluid solid reactions $r_i^{(s)}(\mathbf{x},t)$ is given by

$$r_i^{(s)}[\mathbf{x},\{c_n(\mathbf{x},t)\}] = \sum_m \nu_{im} a_m(\mathbf{x}) k_m \left(1-\Omega_m[\{c_n(\mathbf{x},t)\}]\right), \tag{4.64}$$

with $a_m(\mathbf{x})$ the bulk reactive surface area. Notice that heterogeneous reactions are represented, like homogeneous reactions, through an average source term.

Recall that a reactive transport description in terms of the ADRE assumes that concentration is unique on the support scale V_r and that mass transfer is much faster than the characteristic reaction time scales. As series of studies have investigated the validity of the ADRE (4.63) using volume averaging (Kechagia et al., 2002), pore-network simulations (Meile and Tuncay, 2006; Li et al., 2006) and smoothed particle hydrodynamics (Tartakovsky et al., 2008). These works find consistently discrepancies between reaction rates obtained at the pore scale and their Darcy scale representation (4.63). Battiato et al. (2009) analyzed the conditions under which the ADRE provides a valid description of Darcy scale reactive transport, theoretically, using volume averaging, and numerically, using smoothed particle hydrodynamics. These authors analyze systematically the physical and chemical conditions under which the macroscale description in terms of an ADRE is valid ($Da \ll 1$), and identify the regimes for which a hybrid description is necessary that represents both concentration variability on the support scale as well as the bulk Darcy scale transport properties. To this end, Lichtner and Kang (2007) present a reactive multicontinuum approach that is based on the conceptualization of the medium as consisting of mutiple interaction continua. As in the dual porosity and multirate mass transfer models discussed above, this description quantifies the behavior of the average bulk concentration and represents explicitly concentration

heterogeneity at the support scale. Battiato et al. (2011) develop a (numerical) hybrid method that consists of a coupled system of equations that represents (i) the evolution of the mean concentration through a macroscale reactive transport equation on a coarse grid, (ii) mass transfer between the coarse grid and a fine grid at nodes where the conditions for the macroscale description are not met, (iii) fine scale reactive transport equation at the hybrid node supported with continuum and boundary conditions.

As outlined at the beginning of this section, kinetic rate laws are often determined in the laboratory in well-mixed environments, either batch or flowthrough reactors. Under such conditions, mass transfer limitations and possible localization of geochemical reactions as observed in in-situ measurements do not arise (e.g., Steefel et al., 2005; Li et al., 2006). Li et al. (2008) conducted a thorough experimental and numerical study on the scale dependence of mineral dissolution rates and analyzed the role of concentration gradients in single pores and fractures. These findings again challenge the assumption of well-mixedness necessary for the Darcy-scale reactive transport description (4.63) to be valid.

4.4.2 Darcy to Field Scale

The straightforward generalization of the ADRE approach from the Darcy to the field scale, represents large scale reactive transport by the combination of the macoscale ADE (4.40) and average reaction rates that are formulated in terms of the mean species concentrations

$$\overline{\phi}\frac{\partial \overline{c}_i(\mathbf{x},t)}{\partial t} + \overline{\mathbf{q}} \cdot \nabla \overline{c}_i(\mathbf{x},t) - \nabla \cdot \mathbf{D}^m \nabla \overline{c}_i(\mathbf{x},t) = \overline{\phi}\overline{r}\left[\{\overline{c}_n\}\right] \tag{4.65}$$

We encounter here the same conceptual issues as in the transition from the pore to the Darcy scale. The average reactive transport description (4.40) is valid if the species concentrations are uniform on the macroscopic REV, and mass transfer times on the REV scale are much smaller than the characteristic reaction scale. If these conditions are not fulfilled, the ADRE is only of limited applicability. In fact, it has

been found that macroscale models of reactive transport misrepresent reaction rates in heterogeneous media (e.g., Molz and Widdowson, 1988; MacQuarrie and Sudicky, 1990; Ginn et al., 1995; Kapoor et al., 1997; Gramling et al., 2002). As pointed out above, macrodispersion coefficients overestimate solute dispersion and simulate a homogeneity of the transport system that is not real at practically relevant times (Kitanidis, 1994; Kapoor and Kitanidis, 1998).

Recall that non-Fickian conservative transport observed at the macroscale is related to the fact that concentration is not unique at the macroscopic support scale, or in other words to mass transfer limitations on the support scale. As a consequence, the evolution of average concentration shows memory effects and is quantified by non-local average transport models. Similar scale phenomena have been found for reactive transport. The impact of chemical and physical heterogeneity may lead to large scale reaction rate laws different from those at the local scale. For example, it has been found that reactive transport under heterogenous local equilibrium adsorption properties may be represented on the large scale as a kinetic sorption process (Espinoza and Valocchi, 1997; Dentz and Berkowitz, 2005; Dentz and Castro, 2009).

One may now be tempted to improve the macroscale ADRE along the same lines as for conservative transport, and combine a non-local effective transport model for the average species concentration with reaction rate laws formulated again in terms of the average species concentrations. Even though such a formulation represents the impact of heterogeneity on macroscale transport, it does not represent explicitly the concentration variability at the support scale. Chemical reactions, just like solute mixing, are intrinsically local phenomena, and depend in general on the local scale species concentrations and their gradients.

Thus, also for crossing from the Darcy to the field scale, hybrid models are required that represent the mean behavior of the species concentrations on one hand and that can model explicitly variability in the local species concentrations on the other. As

outlined above and in Section 4.3.2, both the multicontinuum approach (e.g., Lichtner and Kang, 2007; Liu et al., 2008; Donado et al., 2009) and the stochastic-convective approach (e.g., Ginn, 2001) have these attributes and have therefore been used for the modeling of multispecies reactive transport in Darcy-scale heterogenous media.

The multicontinuum approach identifies a connected mobile primary continuum and a suite of secondary continua characterized statistically by a distribution of physical and chemical characteristics, as for example typical mass transfer times, porosity, reactive surface areas and sorption coefficients. The mobile continuum is characterized by a volume averaged mobile concentration that communicates with the fine scale secondary continua through first-order or diffusive mass transfer. Reactive transport is solved for the mobile and each immobile subdomain separately and the average concentrations and reaction rates are determined in terms of the local species concentrations (Lichtner and Kang, 2007; Willmann et al., 2010; Dentz et al., 2011a).

As discussed above, the stochastic-convective model distinguishes solute concentrations between the individual streamtubes, and thus represents small scale concentration variability. In this approach reactive transport is solved for each individual streamtube (e.g., Ginn, 2001; Cirpka and Kitanidis, 2000; Seeboonruang and Ginn, 2006a,b), and therefore local concentration fluctuations can be quantified in the overall reaction behavior. Notice, however, that the streamtubes are typically not connected such that transverse mixing between streamtubes is not represented. Therefore, global mixing may actually be underestimated because concentration gradients between streamtubes cannot be attenuated and therefore may impact on the prediction of the global reaction behavior. Thus, while the macrodispersion approch may be considered a maximum dilution model (Kitanidis, 1994), the stochastic-convective approach represents a minimal mixing model (Robinson and Viswanathan, 2003; Seeboonruang and Ginn, 2006a).

4.5 Multiphase Flow

This section discusses scale effects in multiphase flow through porous media. We focus on the simultaneous flow of two immiscible fluids in a rigid porous matrix. Fluid flow is characterized by the fluid-solid and fluid-fluid interfaces. The presence of interfaces between the fluids leads to phenomena different from the ones observed in single phase flow.

On the pore scale, flow can be described by the Stokes equation (4.3) for each of the two fluids. At the fluid-fluid interface, the flow velocities are continuous, while the fluid pressures in each phase may be different (Marle, 1981), sustained by the surface tension σ at the interface between the two fluids. For two fluids at rest in a capillary, the interaction between the fluids and the solid walls gives the pressure difference at equilibrium by the Young-Laplace equation as

$$\Delta p = \sigma \left(\frac{1}{r_1} + \frac{1}{r_2} \right) \cos(\theta), \tag{4.66}$$

where r_1 and r_2 are the curvature radii of the respective fluids. In a cylindrical capillary, the radii $r_1 = r_2 = r$ are equal to the capillary diameter. The contact angle θ ($0 < \theta < \pi$) is defined as the angle between the capillary wall and the interface between the two fluids. It depends on the surface tensions between the liquids and the liquids and the solid, which are related through the Young-Dupré equation (Bear, 1972; Sahimi, 2011). For $\theta < \pi/2$, the fluid from whose side the angle is measured, is called wetting, for $\theta > \pi/2$ it is called non-wetting. As discussed in Bear (1972), contact angle and interfacial tension depend in general on the direction the interface is moving (capillary hysteresis).

As for single phase flow, coarse graining of the pore-scale flow problem is required to derive effective flow descriptions for practically relevant temporal and spatial scales. This has been undertaken by volume averaging (Hassanizadeh and Gray, 1990), homogenization theory (Bourgeat, 1997), and numerical pore scale flow modeling (Meakin

and Tartakovsky, 2009). The Darcy scale two-phase flow problem then is described by an extension of the Darcy equation for each fluid

$$\mathbf{q}_\alpha = -\frac{k}{\mu_\alpha} k_{r,\alpha} \left(\nabla p_\alpha - \rho_\alpha \mathbf{g} \right), \tag{4.67}$$

where the subscript α denotes the fluid phase, ρ_α its density, p_α its pressure, μ_α its viscosity, and $\mathbf{g}$ is the downward pointing vector of gravity acceleration. Mass conservation for each fluid is described by

$$\phi \frac{\partial S_\alpha}{\partial t} + \nabla \cdot \mathbf{q}_\alpha = 0, \tag{4.68}$$

where S_α denotes the saturation, or volumetric fraction of fluid phase α in the medium; both fluids are assumed to be incompressible such that $\rho_\alpha =$ constant. Here we have $\sum_\alpha S_\alpha = 1$. As pointed out in Bear (1972), this system of equations was proposed by Wyckoff and Botset (1936) and Muskat (1937) as a generalization of the single phase flow description in Darcy scale porous media. Equations (4.67)–(4.68) are complemented by constitutive relationships that relate the pressures in each of the two fluids, and describe the relative saturation $k_{r,\alpha}$ for each fluid. In the simultaneous flow of two fluids, the pore space available for one fluid is limited due to the presence of the other fluid, which therefore reduces its permeability. With this reasoning, relative permeability $k_{r,\alpha}$ is related to fluid saturation S_α. An extensive discussion on the concept of relative permeability and the dependence on fluid saturation can be found in (Bear, 1972).

Capillary pressure $p_c = p_{nw} - p_w$ denotes the difference between the pressures in the wetting and non-wetting fluid phases. This concept is motivated by the pore-scale interfacial pressure difference (4.66) between the two fluids. Capillary pressure is in general related to fluid saturation, $p_c = p_c(S_\alpha)$. As outlined on Marle (1981), for a conic capillary the interface is spherical and fluid saturation may be uniquely related to the interfacial pressure. This is not true anymore for porous media, which are characterized by a complex pore geometry and a distribution of pore length scales.

Capillary hysteresis and pore-scale heterogeneity lead to hysteresis effects in the capillary pressure-saturation relationship, which depends on whether the wetting fluid displaces the non-wetting (imbibition curve) or vice-versa (drainage curve). Furthermore, notice that the Young-Laplace equation (4.66) describes the conditions at the interface at equilibrium. Thus, the simple $p_c(S_\alpha)$ relationship may not be sufficient to describe dynamic phenomena (Das and Mirzaei, 2012; Cueto-Felgueroso and Juanes, 2012). Thus, several authors proposed dynamic relationships between the phase pressures and saturations of the type (see Dahle et al., 2005, and references therein)

$$p_{nw} - p_w = p_c(S_\alpha) + F\left(\frac{\partial S_\alpha}{\partial t}, S_\alpha\right). \tag{4.69}$$

Marle (1981) discusses that (multi-)phase flow in porous media is mainly based on phenomenological macroscale laws that describe fluid flow at the Darcy scale based on macrocopic quantities such as fluid saturations and phase pressures. These laws then are verified or challenged by experiments. This macroscopic approach is contrasted to the microscopic approch that ideally understands porous media flow based on the *elementary laws of visous flow in a pore and from the laws of capillarity.* At the time, *no serious study [had] yet been undertaken of the flow of several fluids.* To date, volume averaging and homogenization theory as well as pore-scale flow simulations have shed new light on the foundations of the Darcy-scale multiphase flow description. Yet many open questions remain (Das and Hassanizadeh, 2005; Cueto-Felgueroso and Juanes, 2012).

In the remainder of this section, we will focus on the quantification of large scale two-phase flow in Darcy-scale porous media. We will rely on the description of two-phase flow through equations (4.68) and (4.67) complemented by the static capillary pressure-saturation relationship $p_{nw} - p_w = p_c(S_\alpha)$, and saturation dependent relative permeability $k_{r,\alpha}(S_\alpha)$. We first focus on the large scale description of two-phase flow in moderately heterogeneous porous media. We present an approach based on stochastic modeling of spatial heterogeneity, which render a non-local large scale flow model. The

front roughening due to spatial heterogeneity can described here in terms of a flow parameter similar to the macrodispersion coefficients discussed above. For transport in strongly heterogeneous media with sharps contrasts in hydraulic conductivity such as fractured media, we review multicontinuum and multirate mass transfer approaches. We then consider the derivation of large scale two-phase flow models through dimensional reduction. Finally, we give an overview over the upscaling of convective mixing in porous media.

4.5.1 Macrodispersion Two-Phase Flow Model

Spatial heterogeneities can lead to an increase in the interfacial area between two fluids, and thus have an impact on the dissolution efficiency between fluid phases. The spreading of the saturation distribution in a homogeneous and a heterogeneous medium is illustrated in Figure 4.10. While the homogeneous model is characterized by a constant saturation value along a cross-section, the heterogeneous model is characterized by a distribution of saturation values, and with larger interface length due to heterogeneity-induced front roughening (Noetinger et al., 2004).

As discussed in Section 4.3.2, dispersive transition zones in solute transport problems have typically been characterized by spatial moments. Due to the qualitative similarity of heterogeneity-induced front roughening, similar approaches have been applied to two-phase flow. Cvetovic and Dagan (1996) and Dagan and Cvetkovic (1996) used Lagrangian perturbation theory in a stochastic modeling approach in order to determine the averaged cumulative recovery of the displacing fluid and the spatial moments of the fluid distribution. They found that spatial heterogeneities cause a dispersive growth of the second moment. Also Zhang and Tchelepi (1999) observed a dispersion effect for horizontal immiscible displacement. Langlo and Espedal (1995) quantified the heterogeneity-induced front dispersion with an effective dispersion coefficient. Their approach was extended by Neuweiler et al. (2003) to quantify the dispersion coefficient

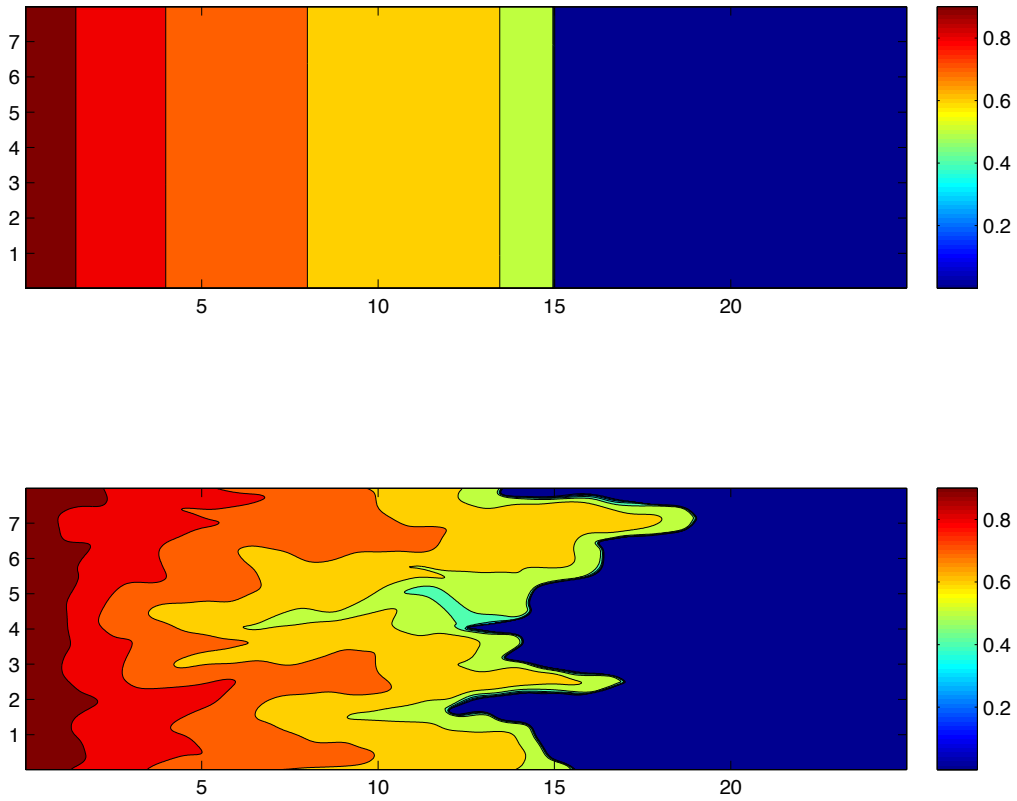

Figure 4.10: Saturation distributions in (top) a homogeneous medium, and (bottom) a heterogeneous medium. The displacing fluid is injected at the left boundary at constant rate. Gravity and capillary effects are disregarded (after Bolster et al., 2009).

analytically, by Bolster et al. (2009) to include temporal fluctuations in the flow field, and Bolster et al. (2011) to account for the impact of gravity and heterogeneity on front spreading. Panfilov and Floriat (2004) use a homogenization approach to quantify the front dispersion in a periodic medium.

In the following, we outline the stochastic-perturbative approach to the quantification of large scale flow in moderately heterogeneous media. As in the context of single phase flow and transport, see Sections 4.2.2 and 4.3.2, the heterogeneous medium is modeled as a realization of an ensemble of random media. A large scale flow equation can then be derived by ensemble averaging of the flow problem. Perturbation theory is used to relate the local scale fluctuations of hydraulic conductivity to the large scale

flow formulation. Medium and fluid are incompressible so that porosity ϕ and phase densities ρ_α are constant.

Quantities that refer to the wetting and non-wetting phases, in the following are marked by the subscript w and nw, respectivley. Incompressibility and mass conservation imply that the divergence of the total specific discharge $\mathbf{Q} = \sum_\alpha \mathbf{q}_\alpha$ is zero, $\nabla \cdot \mathbf{Q} = 0$. Eliminating $\mathbf{q}_{nw}$ from Eq. (4.68) in favor of $\mathbf{Q}$ by using (4.67) gives the two-phase flow problem in the fractional flow formulation (Bear, 1972) for the non-wetting phase as

$$\frac{\partial S_{nw}}{\partial t} + \nabla \cdot \left[\mathbf{Q} f_{nw}(S_{nw}) - \frac{k \Delta \rho_{nw} \mathbf{g}}{\mu_w} g_{nw}(S_{nw}) \right] - \nabla \cdot \left[\frac{k}{\mu_w} g_{nw}(S_{nw}) \nabla p_c(S_{nw}) \right] = 0, \tag{4.70}$$

where $\Delta \rho_{nw} = \rho_w - \rho_{nw}$. We set $\phi = 1$ for simplicity (which is equivalent to rescaling time). The fractional flow function $f_{nw}(S_{nw})$ and modified fractional flow function $g_{nw}(S_{nw})$ are defined by

$$f_{nw}(S_{nw}) = \frac{\lambda_{nw}(S_{nw})}{\lambda_{nw}(S_{nw}) + \lambda_w(S_{nw})}, \qquad g_{nw}(S_{nw}) = k_{r,w}(S_{nw}) f_{nw}(S_{nw}). \tag{4.71}$$

where the phase mobilites are defined by $\lambda_\alpha = k_{r,\alpha}/\mu_\alpha$. Notice that equation (4.70) may be considered a non-linear advection-dispersion equation for the phase separation, in which the second term on the left side represents non-linear advection, the second term non-linear dispersion.

For simplicity, we disregard gravity and set capillary pressure constant in the following. Equation (4.70) then simplifies to the Buckley-Leverett equation

$$\frac{\partial S_{nw}}{\partial t} + \mathbf{Q} \cdot \nabla f_{nw}(S_{nw}) = 0, \tag{4.72}$$

For constant capillary pressure, the total flow velocity $\mathbf{Q}$ satisfies the Darcy equation

$$\mathbf{Q} = -k \Lambda(S_{nw}) \nabla p_{nw}, \qquad \Lambda(S_{nw}) = \frac{k_{r,nw}(S_{nw})}{\mu_{nw}} + \frac{k_{r,w}(S_{nw})}{\mu_w}. \tag{4.73}$$

We focus on the steady displacement of the wetting by the non-wetting as illustrated in Figure 4.10. The total flux at the inflow boundary is prescribed as $\mathbf{Q} = Q_0 \mathbf{e}_1$,

where $\mathbf{e}_1$ is the unit-vector in 1–direction. It can be decomposed into its imposed mean and fluctuations about it, $\mathbf{Q}(\mathbf{x}) = Q_0\mathbf{e}_1 + \mathbf{Q}'$. Substituting the flux decomposition into (4.72), the local scale saturation equation reads as

$$\frac{\partial S_{nw}(\mathbf{x},t)}{\partial t} + Q_0\frac{\partial f_{nw}(S_{nw})}{\partial x_1} + \mathbf{Q}'\cdot\nabla f(S_{nw}) = 0. \tag{4.74}$$

In analogy to the decomposition of total discharge and permeability, we assume that the saturation can be decomposed into its ensemble average $\overline{S}_{nw}$ and fluctuations about it $S_{nw} = \overline{S}_{nw} + S'_{nw}$. Furthermore, assuming that the saturation fluctuations are small, the fractional flow function can be expanded about its mean as $f(S_{nw}) = f(\overline{S}_{nw}) + \frac{df(\overline{S_{nw}})}{d\overline{S_{nw}}}S'_{nw} + \dots$. Using these decompositions in (4.74) and subsequently performing the ensemble average gives the large scale flow equation

$$\frac{\partial \overline{S}_{nw}}{\partial t} + Q_0\frac{\partial f_{nw}(\overline{S}_{nw})}{\partial x_1} = -\nabla\cdot\overline{\mathbf{Q}'S'_{nw}}\frac{df(\overline{S}_{nw})}{d\overline{S}_{nw}}. \tag{4.75}$$

The flux term on the right side depends on the local scale fluctuation of the total flow velocity and phase saturation, and therefore it is not closed. However, by subtracting the average equation (4.75) from the local scale equation (4.75) and disregarding contributions that are quadratic or higher order in the fluctuations, one obtains the following equation for the fluctuations of the phase saturations

$$\frac{\partial S'_{nw}}{\partial t} + Q_0\frac{\partial}{\partial x_1}\frac{df_{nw}(\overline{S}_{nw})}{d\overline{S}_{nw}}S'_{nw} = -\mathbf{Q}'\cdot\nabla f_{nw}(\overline{S}_{nw}). \tag{4.76}$$

This is a linear, closed form equation for S'_{nw} that is based on disregarding higher-order fluctuations of flow velocity and saturation. Therefore, the large scale flow equation (4.75) is closed perturbatively here. Notice, that in the previous section, the Dupuit approximation has been used to close the vertically averaged large scale flow problem.

The linear equation (4.76) can be solved in terms of the associated Green's function $G(\mathbf{x},t|\mathbf{x}',t')$, which solves (4.76) for the initial condition $G(\mathbf{x},t|\mathbf{x}',t') = \delta(\mathbf{x}-\mathbf{x}')$. Thus,

we obtain for S'_{nw} the expression

$$S'_{nw} = -\int_0^t dt' \int d\mathbf{x}' G(\mathbf{x}, t|\mathbf{x}', t')\mathbf{Q}'(\mathbf{x}') \cdot \nabla' f\left[\overline{S}_{nw}(\mathbf{x}', t')\right], \tag{4.77}$$

Inserting (4.77) into (4.75), gives a closed form large scale equation for the average saturation that can be written as the spatially and temporally non-local non-linear advection-dispersion equation

$$\frac{\partial \overline{S}_{nw}}{\partial t} + Q_0 \frac{\partial f(\overline{S}_{nw})}{\partial x_1} - \nabla \cdot \int_0^t dt' \int d\mathbf{x}' \frac{df(\overline{S})}{d\overline{S}_{nw}(\mathbf{x}, t)} \boldsymbol{k}(\mathbf{x}, t|\mathbf{x}', t') \nabla' f\left[\overline{S}_{nw}(\mathbf{x}', t')\right] = 0. \tag{4.78}$$

The impact of the local scale flow fluctuations, and therefore the impact of heterogeneity on large scale flow, is encoded in the kernel function

$$k_{ij}(\mathbf{x}, t|\mathbf{x}', t') = \overline{Q'_i(\mathbf{x}) G(\mathbf{x}, t|\mathbf{x}', t') Q'_j(\mathbf{x}')}. \tag{4.79}$$

Equation (4.78) has a similar structure as (4.70). However, while in (4.70) the (non-local) dispersive flux term originates from the presence of capillary pressure, here it comes from spatial heterogeneity on the Darcy scale. As outlined previously, non-local fluxes typically occur when averaging. The non-linear character of the two-phase problem is preserved during the upscaling excercise. However, in order to close the large scale flow problem, the non-linearity is quasi-decoupled in (4.76) by using perturbation theory, so that S' can be related to the large scale saturation through the Green's function G. Explicit expressions for G can be found in Neuweiler et al. (2003) and Bolster et al. (2009).

In order to quantify the dispersion of the displacement front, Neuweiler et al. (2003) equate the non-local flux term on the right side of (4.78) to

$$\int_0^t dt' \int d\mathbf{x}' \frac{df(\overline{S}_{nw})}{d\overline{S}_{nw}(\mathbf{x}, t)} \boldsymbol{k}(\mathbf{x}, t|\mathbf{x}', t') \nabla' f\left[\overline{S}_{nw}(\mathbf{x}', t')\right] \equiv \mathbf{D}^*(t) \nabla f\left[\overline{S}_{nw}(\mathbf{x}, t)\right], \tag{4.80}$$

which defines the dispersion tensor $\mathbf{D}^*(t)$. A perturbation theory calculation (Neuweiler et al., 2003; Bolster et al., 2009) then gives the following compact expression for the macrodispersion coefficient in flow direction

$$D_{11}^* = \sigma_Y^2 Q_0^2 \int_0^{Q_0 t} \mathrm{d}x_1 C_{11}(x_1), \tag{4.81}$$

where C_{11} denotes the correlation function of Q_1'. It may be approximated by the corelation function for single phase flow as outlined in Neuweiler et al. (2003) and Bolster et al. (2009). Figure 4.11 illustrates the evolution of the front spreading obtained from numerical solution of the two-phase flow problem (4.72) and the analytical expression (4.81).

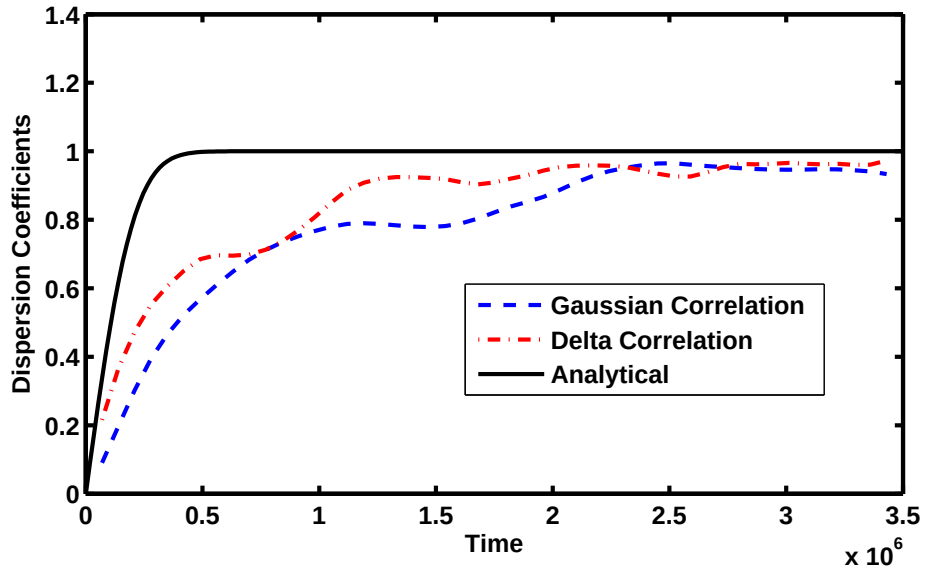

Figure 4.11: Temporal behavior of the dispersion coefficient (4.81) and the evolution of the front width obtained from the numerical solution of the heterogeneous two-phase problem for a Gaussian and Delta autocorrelation functions with $\sigma_Y^2 = 0.5$, normalized by the long-time asymptotic value of (4.81) from (after Bolster et al., 2009).

In summary, the stochastic perturbative approach yields a large scale two-phase flow equation that is characterized by a non-local and non-linear dispersive flux term. The

impact of heterogeneity in permeability leads to a roughening of the interface between the two fluids that can be described by an effective dispersion coefficient. It needs to be noted that dispersion here does not describe mixing, or blending, of the two immiscible fluids, but purely heterogeneity-induced spreading. Thus, the dispersion coefficient and the related interface width serve rather as bulk measure for the interface length.

4.5.2 Multicontinuum Two-Phase Flow Model

The multicontinuum approach for two-phase flow in highly heterogeneous media is in line with the ones reported in Sections 4.2.2 and 4.3.2 for single phase flow and transport, respectively. We consider a highly heterogeneous medium of the type illustrated in Figure 4.3 with clearly delineated mobile and immobile flow regions.

The invading fluid now is the wetting and the displaced the non-wetting phase. We formulate the two-phase flow problem in terms of the saturation of the wetting phase, which here is denoted by $S = S_w$. The two-phase flow problem in the fractional flow formulation reads in terms of the wetting fluid phase as

$$\phi \frac{\partial S}{\partial t} + \nabla \cdot \left[\mathbf{Q} f_w(S) - \frac{k \Delta \rho_w \mathbf{g}}{\mu_{nw}} g_w(S) \right] + \nabla \cdot \left[\frac{k}{\mu_{nw}} g_w(S) \nabla p_c(S) \right] = 0, \tag{4.82}$$

where $\Delta \rho_w = \rho_{nw} - \rho_w$. The fractional flow function $f_w(S)$ and modified fractional flow function $g_w(S)$ for the wetting phase are defined by

$$f_w(S) = \frac{\lambda_w(S)}{\lambda_w(S) + \lambda_{nw}(S)}, \qquad g_w(S) = k_{r,w}(S) f_w(S). \tag{4.83}$$

It is assumed that flow within the matrix blocks is mainly capillary dominated, this means viscous and gravity forces are subdominant in the immobile regions. Parameters, parameter functions and observables that refer to the fracture domain in the following are marked by subscript f, their matrix counterpart by subscript m. Thus, the flow equation (4.82) in the fracture domain reads as

$$\phi_f \frac{\partial S_f}{\partial t} + \nabla \cdot \left[\mathbf{Q}_f f_w(S_f) - \frac{k_f \Delta \rho_w \mathbf{g}}{\mu_{nw}} g_w(S_f) \right] + \nabla \cdot \left[\frac{k_f}{\mu_{nw}} g_w(S_f) \nabla p_{c,f}(S_f) \right] = 0, \tag{4.84}$$

For the matrix domain, one obtains from (4.82) by disregarding viscous and and gravity forces

$$\phi_m \frac{\partial S_m}{\partial t} + \nabla \cdot \left[\frac{k_m}{\mu_{nw}} g_w(S_m) \nabla p_{c,m}(S_m) \right] = 0. \tag{4.85}$$

The conditions at the interface are continuity of flux and pressure, which are expressed by

$$k_f g_w(S_f) \mathbf{n}_{fm} \cdot \nabla p_{c,f}(S_f) = k_m g_w(S_m) \mathbf{n}_{fm} \cdot \nabla p_{c,m}(S_m), \tag{4.86}$$

$$p_{c,f}(S_f) = p_{c,m}(S_m) \tag{4.87}$$

for $\mathbf{x} \in \partial\Omega_{fm}$, where $\partial\Omega_{fm}$ denotes the fracture-matrix interface, and $\mathbf{n}_{fm}$ the unit vector perpendicular to the interface.

Using a multiscale expansion, Tecklenburg et al. (2013) derive the following large scale flow model for the (volume) averaged saturation $\overline{S}_f$

$$\begin{aligned} &\varphi_f \phi_f \frac{\partial \overline{S}_f}{\partial t} + \nabla \cdot \left[\varphi_f \overline{\mathbf{Q}}_f f_w(\overline{S}_f) - \frac{\varphi_f k_f \Delta\rho_w \mathbf{g}}{\mu_{nw}} g_w(S_f) \right] + \nabla \cdot \left[\frac{\varphi_f k_f}{\mu_{nw}} g_w(\overline{S}_f) \nabla p_{c,f}(\overline{S}_f) \right] \\ &- \nabla \cdot \varphi_f \mathbf{D}^* \nabla f_w(\overline{S}_f) = -\varphi_m \phi_m \frac{\partial \overline{S}_m}{\partial t}, \end{aligned} \tag{4.88}$$

where $\overline{\mathbf{Q}}_f$ is the average total flow in the facture domain. As in Section 4.2.2, φ_f and φ_m denote the volume fractions of the fracture and matrix domains. The macrodispersion tensor $\mathbf{D}^*$ can be identified with the one defined in (4.80). The average saturation $\overline{S}_m$ in the matrix domain is given by the volume average of S_m, which is determined from (4.85) with the boundary condition

$$p_{c,m}(S_m) = p_{c,f}(\overline{S}_f) \tag{4.89}$$

for $\mathbf{y} \in \partial\Omega_m$; $\partial\Omega_m$ denotes the boundary of the matrix domain, and $\mathbf{y}$ the position vector in the coordinate system attached to the matrix domain.

The closed system of equations constituted by equations (4.85) with the boundary condition (4.89) and (4.88) constitute the multicontinuum large scale flow model for

the average fracture saturation $\overline{S}_f$. Note that the resulting flow model depends on the non-linear diffusion properties between the mobile and immobile zones as expressed by (4.85) and (4.89). Thus, we seek to simplify the capillary diffusion problem (4.85) thus and relate it back to the single phase flow problem. To this end, we expand (4.85) in the form

$$\phi_m \frac{\partial S_m}{\partial t} - \nabla_y \cdot [\mathcal{D}_c' \nabla_y S_m] = 0, \qquad \mathcal{D}_c' = \frac{k_m}{\mu_{nw}} g_w(S_m) \frac{dp_{c,m}(S_m)}{dS_m}, \tag{4.90}$$

where $\mathcal{D}_c'$ represents the non-linear capillary diffusion coefficient (McWorther and Sunada, 1990). We approximate $\mathcal{D}_c'$ by a suitably chosen constant value such that $\mathcal{D}_c' = \mathcal{D}_c = \text{constant}$ (Tecklenburg et al., 2013). This approximation may appear quite drastic. However, we are not so much interested in the distribution of saturation inside the immobile region, as in the average matrix saturation $\overline{S}_m$. Schmid and Geiger (2012) determined the characteristic time scale τ_c for capillary diffusion into a matrix block of typical size ℓ_m in terms of the capillary flow properties within the matrix. Thus, the constant average capillary diffusion coefficient can is estimated as $\mathcal{D}_c = \ell_m^2/(2\tau_c)$. With this simplification, (4.70) reduces to a linear diffusion equation that can be solved by the method of Green's functions. As a matter of fact, the immobile flow problem is similar to the corresponding matrix problems for single phase flow transport, with the difference that the diffusion coefficient $\mathcal{D}_c$ here is determined from the capillary flow properties in the matrix, and that the matrix saturation at the boundary of the matrix domain is given implicitly in terms of the average fracture saturation by (4.89).

For a uniform initial saturation S_{m0} inside the matrix, S_m can be determined in terms of the Green's function that solves the diffusion problem (4.90) in the matrix domain for a unit Delta pulse on the matrix boundary. The case of heterogeneous distributions is detailed in Tecklenburg et al. (2013). Finally, one obtains for the average saturation in the immobile zones

$$\overline{S}_m = S_{m0} - S_{m0} \int_0^t dt' g_m(t') + \int_0^t dt' g_m(t - t') S_{mb}(t'). \tag{4.91}$$

where we defined the boundary saturation S_{mb} from (4.89) as $S_{mb} = p_{c,m}^{-1}[p_{c,f}(\overline{S}_f)]$. Inserting this expression into (4.88) gives a single equation large scale flow model (Geiger et al., 2013; Tecklenburg et al., 2013)

$$\varphi_f \phi_f \frac{\partial \overline{S}_f}{\partial t} + \nabla \cdot \left[\varphi_f \mathbf{Q} f_w(\overline{S}_f) - \frac{\varphi_f k_f \Delta \rho_w \mathbf{g}}{\mu_{nw}} g_w(S_f) \right] + \nabla \cdot \left[\frac{\varphi_f k_f}{\mu_{nw}} g_w(\overline{S}_f) \nabla p_{c,f}(\overline{S}_f) \right] - \nabla \cdot \varphi_f \mathbf{D}^* \nabla f_w(\overline{S}_f) = \Gamma(t), \tag{4.92}$$

where the source term $\Gamma(t)$ is given by

$$\Gamma(t) = -\varphi_m \phi_m \frac{d}{dt} \int_0^t dt' g_m(t - t') S_{mb}(t') + \varphi_m \phi_m S_{m0} g_m(t). \tag{4.93}$$

In the absence of capillary and gravity forces in the fracture, and for a linear fractional flow function $f_w(\overline{S}_w) = \overline{S}_w$, the large scale flow model is equal to the corresponding MRMT solute transport model.

The large scale model (4.88) can be readily generalized to account for a distribution of immobile continua characterized by different geometries and hydraulic properties. In this case, the source term $\Gamma(t)$ is generalized to $\Gamma(t) = \sum_i \varphi_{m,i} \phi_{m,i} g_{m,i}(t)$, where $\varphi_{m,i}$ and $\phi_{m,i}$ are volume fraction and porosity of the ith immobile continuum. The memory functions $g_{m,i}(t)$ quantify the mass exchange between the ith immobile continuum and the mobile continuum.

Multicontinuum models have been used for the large scale modeling of unsaturated flow and for the simulation of water-oil diplacement for simulating oil recovery from fractured reservoirs. For the modeling of unsaturated flow, Simunek et al. (2003) and Gerke (2006) distinguish multi-permeability and multi-porosity approaches. In the former, all the continua, characterized by different hydraulic properties, are mobile, and connected through a mass transfer term, while the latter distinguish a mobile and a set of immobile continua. In the oil and gas community such models are termed dual-permeability and dual-porosity models, respectively (Kazemi et al., 1976). Di Donato et al. (2007) present a multirate mass transfer model that has certain similarities with

the one described above. These authors consider first-order mass transfer between the fracture and the matrix, similar to the one reported in Section 4.2.2. It is assumed, however, that the mass flux between the fracture and matrix domains is independent on the fracture saturation, but depends only on the difference between the maximum matrix saturation and the actual saturation.

4.5.3 Vertically Integrated Models

Vertically integrated large scale models seek to simplify the full two-phase flow problem and express the large scale flow problem in terms of the vertically integrated observables. This implies the projection, or compression of the original dynamic equation, and subsequent modeling of flux terms that are in general depend on the small scale details of the flow problems. This is a well-known problem in flow and transport upscaling. The macrodispersion approach reported above for the two-phase flow problem, and in Section 4.3.2 for transport, models the non-local flux terms by the macrodispersion closure $\overline{\mathbf{u}'c} = \mathbf{D}^m \nabla \bar{c}$, where $\mathbf{u}'$ is a velocity fluctuation, $\mathbf{D}^m$ a macroscale dispersion tensor, and $\bar{c}$ an average concentration. The multicontinuum approaches for flow and transport detailed above and in Sections 4.2.2 and 4.3.2 represents the fluxes between the small and large scales through a memory function that is determined by the solution of the small scale flow or transport problem.

Large scale averaged models do not resolve variability along the vertical, which, however, is needed to model the fluxes and relate them to the large scale variables. Nordbotten and Celia (2012) provide an approach based on compression and reconstruction of features, which we want to briefly summarize in the following. These authors employ an heterogeneous multiscale method, which provides a methodological framework to relate the incomplete large scale, or coarse scale model to the small scale, or fine scale model and thus close the coarse scale description. This approach defines a compression operator $\mathcal{C}$, that projects the fine scale on the coarse scale variables,

and a reconstruction operator $\mathcal{R}$ that approximates the fine scale variable based on the coarse variable. Consistency requires that $\mathcal{C}\mathcal{R} = \mathbb{I}$ with $\mathbb{I}$ the identity operator. The reverse is in general not true, $\mathcal{R}\mathcal{C} \neq \mathbb{I}$ because the reconstruction in general provides an approximation to the true fine scale variable.

The compression operator $\mathcal{C}$ may represent a spatial integration, or projection of a characteristic value of the small scale variable. The former applies in the definition of coarse scale phase saturation

$$\overline{S}_\alpha = \mathcal{C}_{S_\alpha} S_\alpha = \int_{\zeta_B}^{\zeta_T} dx_3 S_\alpha. \tag{4.94}$$

In the following, the subscript marks the variable to which compression and reconstruction are applied. The reconstructed saturation is denoted by

$$\hat{S}_\alpha = \mathcal{R}_{S_\alpha} \overline{S}_\alpha. \tag{4.95}$$

For the compression of pressure the second option applies. As emphasized by Nordbotten and Celia (2012), pressure is not an additive quantity, and it is in general not a independent on the vertical position. It is assumed for the following that the Dupuit assumption is valid, this means that flow is predominantly horizontal, $\mathbf{e}_3 \cdot \mathbf{q}_\alpha \approx 0$. Coarse phase pressure is defined by projection as

$$\overline{p}_\alpha = \mathcal{C}_{p_\alpha} p_\alpha = p_\alpha(x_3 = \zeta_0) \tag{4.96}$$

with ζ_0 a reference height. The reconstruction operator $\mathcal{R}_{p_\alpha}$ is obtained immediately as

$$\mathcal{R}_{p_\alpha} \overline{p}_\alpha = \overline{p}_\alpha - \rho_\alpha g(x_3 - \zeta_0). \tag{4.97}$$

For simplicity, we consider a domain with horizontal bottom and top boundaries at $x_3 = \zeta_B$ and $x_3 = \zeta_T$. Vertical averaging of (4.68) gives

$$\phi \overline{S}_\alpha + \nabla_\parallel \cdot \overline{\mathbf{q}}_\alpha = 0, \tag{4.98}$$

where zero flow is assumed at the horizontal boundaries, and porosity ϕ is assumed to be constant. The coarse phase saturations satisfy $\sum_\alpha \overline{S}_\alpha = 1$. The subscript $\|$ denotes the horizontal direction. The fine scale flux $\mathbf{q}_\alpha$ is given by (4.67). Notice that (4.98) is not closed because $\overline{\mathbf{q}}_\alpha$ depends on the fine scale saturations through relative permeability $k_{r,\alpha}$. The equation can be closed subject to a suitable saturation reconstruction, such that the fine scale saturation can be related to the coarse saturation via (4.95). Nordbotten and Celia (2012) derive a reconstruction operator based on the Dupuit reconstruction (4.97) and the saturation dependence of capillary pressure. Based on a unique relation between capillary pressure and saturation, one may write

$$S_\alpha = p_c^{-1}(p_{nw} - p_w). \tag{4.99}$$

Using the Dupuit reconstruction (4.97), the pressure difference between the non-wetting and wetting fluids can be approximated by $p_{nw} - p_w \approx \overline{p}_{nw} - \overline{p}_w - (\rho_{nw} - \rho_w)g(x_3 - \zeta_0)$. This gives the reconstructed saturation as

$$\hat{S}_\alpha = p_c^{-1}\left[\overline{p}_{nw} - \overline{p}_w - (\rho_{nw} - \rho_w)g(x_3 - \zeta_0)\right]. \tag{4.100}$$

The compression of the reconstructed phase saturation $\hat{S}_\alpha$ gives the coarse saturation

$$\overline{S}_\alpha = \mathcal{C}_{S_\alpha}\hat{S}_\alpha = \mathcal{C}_{S_\alpha}p_c^{-1}\left[\overline{p}_{nw} - \overline{p}_w - (\rho_{nw} - \rho_w)g(x_3 - \zeta_0)\right]. \tag{4.101}$$

This follows from the consistence requirement mentioned above. The coarse saturation can be shown (Nordbotten and Celia, 2012) to be monotone and invertible in the pressure difference $\overline{p}_{nw} - \overline{p}_w$, such that a coarse capillary pressure can be defined as

$$\overline{p}_c(\overline{S}_\alpha) = \overline{p}_{nw} - \overline{p}_w. \tag{4.102}$$

Thus, capillary pressure can be reconstructed as a function of the coarse phase saturation as

$$\hat{p}_c(\hat{S}_\alpha) = \overline{p}_c(\overline{S}_\alpha) - (\rho_{nw} - \rho_w)g(x_3 - \zeta_0), \tag{4.103}$$

and therefore, the reconstruction of the phase saturation $\hat{S}_\alpha$ can now be related to the coarse phase saturation through

$$\hat{S}_\alpha = \mathcal{R}_{S_\alpha}\overline{S}_\alpha \equiv p_c^{-1}\left[\overline{p}_c(\overline{S}_\alpha) - (\rho_{nw} - \rho_w)g(x_3 - \zeta_0)\right]. \tag{4.104}$$

The coarse grained Darcy flux $\overline{q}_\alpha$ can then be written in terms of the coarse grained variables as (Nordbotten and Celia, 2012)

$$\overline{q}_\alpha = \int_{\zeta_B}^{\zeta_T} dx_3 \mathbf{e}_\parallel \cdot \mathbf{q}_\alpha = \int_{\zeta_B}^{\zeta_T} dx_3 k \frac{k_{r,\alpha}(\mathcal{R}_{S_\alpha}\overline{S}_\alpha)}{\mu_\alpha} \nabla_\parallel \mathcal{R}_{p_\alpha}\overline{p}_\alpha. \tag{4.105}$$

One may now define the integrated permeability and coarse scale mobilities as

$$\overline{k} = \int_{\zeta_B}^{\zeta_T} dx_3 k, \qquad \overline{\lambda}_\alpha(\overline{S}_\alpha) = \overline{k}^{-1} \int_{\zeta_b}^{\zeta_T} dx_3 k \frac{k_{r,\alpha}(\mathcal{R}_{S_\alpha}\overline{S}_\alpha)}{\mu_\alpha}. \tag{4.106}$$

Thus, the equation for the coarse saturation $\overline{S}_\alpha$ now reads as

$$\phi \frac{\partial \overline{S}_\alpha}{\partial t} - \nabla_\parallel \cdot \left[\overline{k}\, \overline{\lambda}_\alpha(\overline{S}_\alpha)\nabla_\parallel \overline{p}_\alpha\right] = 0. \tag{4.107}$$

This equation, together with the coarse capillary pressure $\overline{p}_c(\overline{S}_\alpha)$ constitute a closed large scale flow model for the coarse phase saturations. This particular model assumes vertical equilibrium. Nordbotten and Celia (2012) discuss simplified models derived from this approach, and also consider generalizations that relax the assumptions of vertical equilibrium, and immiscibility, and incompressibility of the two fluids.

4.5.4 Convective Mixing

The previous sections described modeling approaches to quantify the large scale features of the flow of two immiscible fluids. In this section, we consider the mixing of the phases due to dissolution at the interface and the subsequent occurrence of convective instabilities. Dissolution of CO_2 in the formation water, and possible subsequent geochemical reactions are mechanisms that increase the storage safety. After injection, the buoyant CO_2 will spread and migrate laterally as a gravity current relative to

the denser ambient brine. As CO_2 migrates, dissolution takes place in the interphase with the brine. The CO_2-brine mixture is denser than either of the pure fluids which results in an unstable density stratification. This configuration of fluids triggers a Rayleigh-Bénard hydrodynamic instability known as convective mixing that enhances the dissolution of CO_2.

Onset of convection The time for the onset of convection is a critical factor in the CO_2 dissolution problem. At the critical time convection starts to dominate over diffusion and dissolution grows. The dissolution of CO_2 on top of the formation water leads to an unstable boundary-layer problem analogous to the one found when a fluid is overlaid by a cold boundary (Rees et al., 2008). Following this analogy, CO_2 dissolution is conceptualized in a semi-infinite domain with an impervious top boundary, at which concentration is prescribed equal to CO_2 solubility. The brine is assumed incompressible, the Boussinesq approximation valid and the porous medium homogeneous.

Under these assumptions, the critical time $t_c \propto D(\frac{\phi\mu}{k\Delta\rho g})^2$ (Riaz et al., 2006; Hassanzadeh et al., 2007). The coefficient of proportionality depends on the specific stability analysis method. Dominant mode analysis (Ben et al., 2002; Riaz et al., 2006) gives the largest coefficients, and methods which use a white noise initial condition (Foster, 1965; Caltagirone, 1980; Ennis-King and Paterson, 2005) the lowest. It is found (Slim and Ramakrishnan, 2010) that instabilities only happen for Rayleigh-Darcy numbers $\mathcal{R}$ larger than 32.5. The obtained critical time is layer-thickness dependent for $32.5 < \mathcal{R} < 75$. This limitation disappears if the underlying fluid is allowed to cross the top boundary. All the stability analysis methods overestimate the time for the onset of convection Slim and Ramakrishnan (2010) which can be attributed to the use of physically unrealistic perturbations (Daniel et al., 2013; Tilton et al., 2013).

The time for the onset fo convection is also very sensitive to the conceptual model. More realistic models that include heterogeneity in the permeability field (Xu et al.,

2006; Rapaka et al., 2009) or hydrodynamic dispersion (Hidalgo and Carrera, 2009) predict shorter times for the convection to appear. However, when chemical reactions that consume carbon are taken into account (Andres and Cardoso, 2011; Ghesmat et al., 2011), the time for the onset of convection increases because the boundary layer stabilizes.

Convective mixing and characteristic scales Once convection has developed, the flow is characterized by a fingering pattern as illustrated in Figure 4.12. The dissolution rate during this regime is approximately constant and larger than the one due to purely diffusive dissolution (Kneafsey and Pruess, 2010). A heuristic analysis of the system suggests that the dissolution flux should be scale free, that is, independent of the Rayleigh number Ra (Hidalgo and Carrera, 2009; Slim and Ramakrishnan, 2010). Numerical simulations in 2D (Riaz et al., 2006; Hidalgo and Carrera, 2009) and 3D (Pau et al., 2010) support this hypothesis. However, experimental data obtained using analogue fluid systems suggest a $Ra^{4/5}$ scaling of the dissolution fluxes (Neufeld et al., 2010; Backhaus et al., 2011). The scaling of the dissolution fluxes can be studied through the evolution of the scalar dissipation rate, a magnitude often easier to compute. This method shows that, when the Darcy-Boussinesq model is assumed, there is no dependence of the dissolution flux on Ra (Hidalgo et al., 2012). Similar results have been obtained for 3D simulations (Fu et al., 2013). Therefore the observed non-linear scaling has yet to be explained using effects not present in the traditional model.

Dissolution flux plays a major role in the large scale dynamics of CO_2 migration. As the CO_2 dissolves in the system, the buoyant gravity current slows down and eventually is totally arrested (MacMinn and Juanes, 2013). The behavior of the convection-driven dissolution fluxes presents an intermittent behavior linked to finger growth and merging (Slim et al., 2013). Ultimately, the dissolution flux decreases as the system becomes saturated (Hidalgo et al., 2013). The nature of the convection shutdown depends on the system considered. For 2D box models the flux decays as $\approx t^{-(n+1)/n}$ where n is an

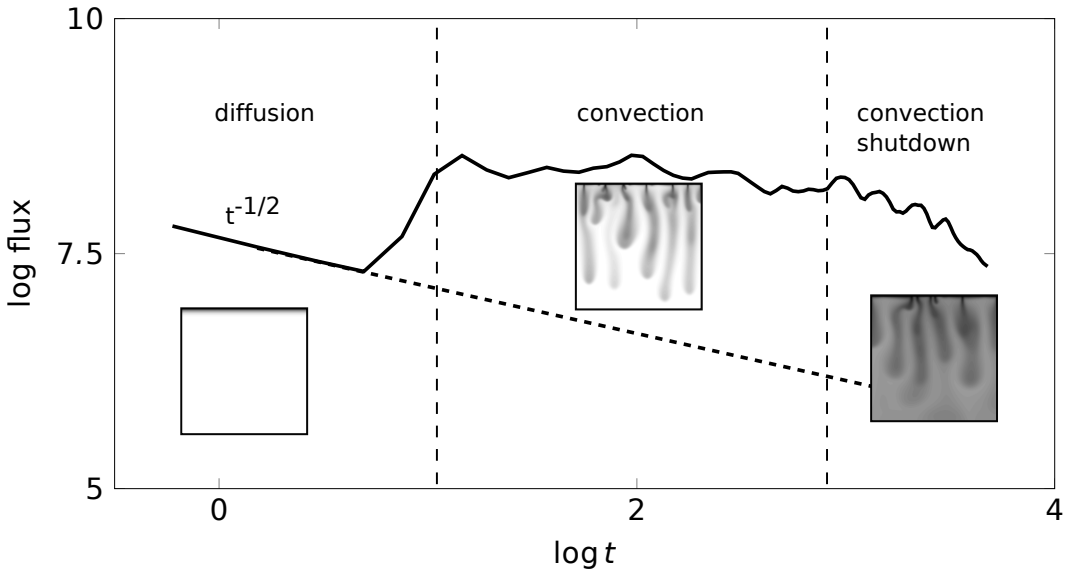

Figure 4.12: Log dissolution flux versus log-time in arbitrary dimensionless units displaying the three main stages of CO_2 dissolution. At the begining CO_2 dissolves into brine through diffusion. The flux decays as $t^{-1/2}$. After the onset of convection the dissolution flux increases sharply. Convection dominated flux remains constant until the underlying brine saturates and the CO_2 flux is shutdown. The three insets show snapshots of the CO_2-brine system representative of the three regimes.

exponent that characterizes the dependence of density with the concentration (Hewitt et al., 2013). However if the dynamics of the CO_2 gravity current is considered flux, decays first diffusively and later sub-diffusively (Szulczewski et al., 2013).

Heterogeneity and chemical reactions have an impact on dissolution. The presence of horizontal obstacles in the aquifer decreases the magnitud of dissolution fluxes (Elenius and Gasda, 2013). The magnitude of the reduction depends on the size and distribution of the barriers. Moderate chemical reactions inhibit finger growing but favor tip splitting. This enhances convection and increases the dissolution flux. With increasing efficiency of chemical reactions, finger formation is suppressed and dissolution is controlled by diffusion (Andres and Cardoso, 2012).

Bibliography

Acharya, R., A., V., Werth, C., and Willingham, T. (2007). Pore-scale simulation of dispersion and reaction along a transverse mixing zone in two-dimensional porous media. *Water Resour. Res.*, 43:W10435.

Adams, E. E. and Gelhar, L. W. (1992). Field study of dispersion in a heterogeneous aquifer, 2. Spatial moment analysis. *Water Resour. Res.*, 28(12):3293–3308.

Andres, J. T. H. and Cardoso, S. S. S. (2011). Onset of convection in a porous medium in the presence of chemical reaction. *Phys. Rev. E*, 83(4):046312.

Andres, J. T. H. and Cardoso, S. S. S. (2012). Convection and reaction in a diffusive boundary layer in a porous medium: Nonlinear dynamics. *Chaos: An Interdisciplinary Journal of Nonlinear Science*, 22(3):037113.

Aris, R. (1956). On the dispersion of a solute in a fluid flowing through a tube. *Proc. R. Soc. London A*, 235:67–77.

Backhaus, S., Turitsyn, K., and Ecke, R. E. (2011). Convective instability and mass transport of diffusion layers in a hele-shaw geometry. *Physical Review Letters*, 106(10):104501.

Barenblatt, G. I., Zheltov, Y. P., and Kochina, I. N. (1960). Basic concepts in the theory of seepage of homogeneous fluids in fissurized rocks. *J. Applied Mathematics and Mechanics (PMM)*, 24:1286–1303.

Batchelor, G. K. (1949). Diusion in a eld of homogeneous turbulence I, Eulerian analysis. *Austral. J. Sci. Res.*, 2:437–450.

Batchelor, G. K. (1952). Diusion in a eld of homogeneous turbulence ii, the relative motion of particles. *Proc. Camb. Phil. Soc.*, 48:345–362.

Battiato, I., Tartakovsky, D. M., Tartakovsky, A. M., and Scheibe, T. (2009). On breakdown of macroscopic models of mixing-controlled heterogeneous reactions in poroous media. *Adv. Water Resour.*, 32:1664–1673.

Battiato, I., Tartakovsky, D. M., Tartakovsky, A. M., and Scheibe, T. D. (2011). Hybrid models of reactive transport in porous and fractured media. *Adv. Water Res.*, 34:1140–1150.

Bear, J. (1972). *Dynamics of fluids in porous media*. American Elsevier, New York.

Beckie, R., Aldama, A. A., and Wood, E. F. (1996). Modeling the large-scale dynamics of saturated groundwater flow using spatial-filtering theory: 1. theoretical development. *Water resources research*, 32(5):1269–1280.

Ben, Y., Demekhin, E. A., and Chang, H.-C. (2002). A spectral theory for small-amplitude miscible fingering. *Physics of Fluids*, 14(3):999.

Benson, D. A., Wheatcrat, S. W., and Meerschaert, M. M. (2000). Application of a fractional advection-dispersion equation. *Water Resour. Res.*, 36:1403–1421.

Berkowitz, B., Cortis, A., Dentz, M., and Scher, H. (2006). Modeling non-fickian transport in geological formations as a continuous time random walk. *Rev. Geophys.*, 44:RG2003.

Berkowitz, B. and Scher, H. (1997). Anomalous transport in random fracture networks. *Phys. Rev. Lett.*, 79(20):4038–4041.

Bijeljic, B. and Blunt, M. J. (2006). Pore-scale modeling and continuous time random walk analysis of dispersion in porous media. *Water Resour. Res.*, 42:W01202.

Bolster, D., Dentz, M., and Carrera, J. (2009). Effective two-phase flow in heterogeneous media under temporal pressure fluctuations. *Water Resour. Res.*, 45:W05408.

Bolster, D., Neuweiler, I., Dentz, M., and Carrera, J. (2011). The impact of buoyancy on front spreading in heterogeneous porous media in twophase immiscible flow. *Water Resour. Res*, 47:W02508.

Bourgeat, A. (1997). *Homogenization and Porous Media*, chapter 5, pages 95–127. Springer.

Brenner, H. (1980). Dispersion resulting from flow through spatially periodic porous media. *Proc. Roy. Soc. A*, 297:81–133.

Brinkman, H. C. (1949). A calculation of the viscous force exerted by a flowing fluid on a dense swarm of particles. *Appl. Sci. Res.*, 1:27–34.

Bronstert, A., Carrera, J., Leavesley, G., and Mölders, N. (2005). *Scale Issues*, pages 21–43. Springer.

Caltagirone, J.-p. (1980). Stability of a saturated porous layer subject to a sudden rise in surface temperature: comparison between the linear and energy methods. *The Quarterly Journal of Mechanics and Applied Mathematics*, 33(1):47–58.

Carrera, J. (1993). An overview of uncertainties in modelling groundwater solute transport. *J. Cont. Hydrol.*, 13:23–84.

Carrera, J., Sánchez-Vila, X., Benet, I., Medina, A., Galarza, G., and Guimerà, J. (1998). On matrix diffusion: formulations, solution methods, and qualitative effects. *Hydrogeology Journal*, 6:178–190.

Cirpka, O. A. and Kitanidis, P. K. (2000). An advective-dispersive streamtube approach for the transfer of conservative tracer data to reactive transport. *Water Resour. Res.*, 36:1209–1220.

Cueto-Felgueroso, L. and Juanes, R. (2012). Macroscopic phase-field model of partial wetting: bubbles in a capillary tube. *Phys. Rev. Lett.*, 108:144502.

Cunningham, J. A., Werth, C. J., Reinhard, M., and Roberts, P. V. (1997). Effects of grain-scale mass transfer on the transport of volatile organics through sediments: 1, model developments. *Water Resour. Res.*, 33:2713–2726.

Cushman, J. H., Bennethum, L. S., and Hu, B. X. (2002). A primer on up-scaling tools for porous media. *Adv. Water Resour.*, 25:1043–1067.

Cushman, J. H. and Ginn, T. R. (1993). Nonlocal dispersion in media with continuously evolving scales of heterogeneity. *Transp. Porous Media*, 13(1):123–138.

Cushman, J. H. and Ginn, T. R. (2000). Fractional advection-dispersion equation: A classical mass balance with convolution–Fickian flux. *Water Resour. Res.*, 36:3763–3766.

Cvetovic, V. and Dagan, G. (1996). Reactive transport and immiscible flow in geological media. ii. applications. *Proc. R. Soc. Lond. A*, 452:202–328.

Dagan, G. (1984). Solute transport in heterogenous porous formations. *J. Fluid Mech.*, 145:151–177.

Dagan, G. (1986). Statistical theory of gtoundwater flow and transport: Pore to laboratory, laboratory to formation and formation to regional scale. *Water Resour. Res.*, 22:120S–134S.

Dagan, G. (1988). Time-dependent macrodispersion for solute transport in anisotropic heterogeneous aquifers. *Water Resour. Res*, 24(9):1491–1500.

Dagan, G. (1989). *Flow and Transport in Porous Formations*. Springer, New York.

Dagan, G. and Bressler, E. (1979). Solute dispersion in unsaturated soil at field scale, i, theory. *Soil Sci. Soc. Am. J.*, 43:461–466.

Dagan, G. and Cvetkovic, V. (1996). Reactive transport and immiscible flow in geological media i general theory. *P. Roy. Soc. Lond. A*, 452:285–301.

Dahle, H. K., Celia, M. A., and Hassanizadeh, S. M. (2005). Bundle-of-tubes model for calculating dynamic effects in the capillary-pressure saturation relationship. *Transp. Porous Med.*, 58:5–22.

Daniel, D., Tilton, N., and Riaz, A. (2013). Optimal perturbations of gravitationally unstable, transient boundary layers in porous media. *J. Fluid Mech.*, 727:456–487.

Das, D. B. and Hassanizadeh, S. M., editors (2005). *Upscaling Multiphase Flow in Porous Media*. Springer.

Das, D. B. and Mirzaei, M. (2012). Dynamic effects in capillary pressure reationships for two-phase flow in porous media: expeirments and numerical analyses. *AIChE J.*, 58:3891–3903.

De Dreuzy, J. R., Carrera, J., Dentz, M., and Le Borgne, T. (2012). Time evolution of mixing in heterogeneous porous media. *Water Resour. Res.*, 48:W06511.

De Simoni, M., Carrera, J., Sánchez-Vila, X., and Guadagnini, A. (2005). A procedure for the solution of multicomponent reactive transport problems. *Water Resour. Res.*, 41:2005WR004056.

De Simoni, M., Sánchez-Vila, X., Carrera, J., and Saaltink, M. W. (2007). A mixing ratios-based formulation for multicomponent reactive transport. *Water Resour. Res.*, 43:W07419.

Dean, D. S., Drummond, I. T., and Horgan, R. R. (2007). Effective transport properties for diffusion in random media. *J. Stat. Mech.*, 7:P07013.

Delay, F., Ackerer, P., and Danquigny, C. (2005). Simulating solute transport in porous or fractured formations using random walk particle tracking. *Vadose Zone J.*, 4:360–379.

Dentz, M. and Berkowitz, B. (2003). Transport behavior of a passive solute in continuous time random walks and multirate mass transfer. *Water Resour. Res.*, 39(5):1111.

Dentz, M. and Berkowitz, B. (2005). Exact effective transport dynamics in a one-dimensional random environment. *Phys. Rev. E*, 72(3):031110.

Dentz, M. and Castro, A. (2009). Effective transport dynamics in porous media with heterogeneous retardation properties. *Geophys. Res. Lett.*, 36:L03403.

Dentz, M., Gouze, P., and Carrera, J. (2011a). Effective non-local reaction kinetics for transport in physically and chemically heterogeneous media. *J. Cont. Hydrol.*, 120-121:222236.

Dentz, M., Kinzelbach, H., Attinger, S., and Kinzelbach, W. (2000). Temporal behavior of a solute cloud in a heterogeneous porous medium, 1, point-like injection. *Water Resour. Res.*, 36(12):3591–3604.

Dentz, M., LeBorgne, T., Englert, A., and Bijeljic, B. (2011b). Mixing, spreading and reaction in heterogeneous media: A brief review. *J. Cont. Hydrol.*, 120-121:1–17.

Di Donato, G., Lu, H. Y., Tavassoli, Z., and Blunt, M. J. (2007). Multirate-transfer dual-porosity modeling of gravity drainage and imbibition. *SPE Journal*, 12(1):77–88.

Donado, L. D., Sanchez-Vila, X., Dentz, M., Carrera, J., and Bolster, D. (2009).

Multi-component reactive transport in multi-continuum media. *Water Resour. Res.*, 45:W11402.

Edwards, D. A., Shapiro, M., and Brenner, H. (1993). Dispersion and reaction in two-dimensional model porous media. *Phys. Fluids A*, 5:837–848.

Elenius, M. T. and Gasda, S. E. (2013). Convective mixing in formations with horizontal barriers. *Advances in Water Resources*, 62:499–510.

Ennis-King, J. and Paterson, L. (2005). Role of convective mixing in the long-term storage of carbon dioxide in deep saline formations. *SPE Journal*, 10(3).

Espinoza, C. and Valocchi, A. J. (1997). Stochastic analysis of one-dimensional transport of kinetically adsorbing solutes in chemically heterogeneous aquifers. *Water Resour. Res.*, 33(11):2429–2445.

Foster, T. D. (1965). Stability of a homogeneous fluid cooled uniformly from above. *Physics of Fluids*, 8(7):1249.

Fu, X., Cueto-Felgueroso, L., and Juanes, R. (2013). Pattern formation and coarsening dynamics in three-dimensional convective mixing in porous media. *Philosophical Transactions of the Royal Society A: Mathematical,Physical and Engineering Sciences*, 371(2004).

Geiger, S., M., D., and Neuweiler, I. (2013). A novel multirate dual-porosity model for improved simulation of fractured and multiporosity reservoirs. *SPE J.*, 18:670–684.

Gelhar, L. (1993). *Stochastic Subsurface Hydrology*. Prentice Hall, Englewood Cliffs, NJ.

Gelhar, L. W. and Axness, C. L. (1983). Three-dimensional stochastic analysis of macrodispersion in aquifers. *Water Resour. Res.*, 19(1):161–180.

Gelhar, L. W., Welty, C., and Rehfeldt, K. R. (1992). A critical review of data on field-scale dispersion in aquifers. *Water Resour. Res.*, 28(7):1955–1974.

Gerke, H. H. (2006). Preferential flow descriptions for structured soils. *Journal of Plant Nutrition and Soil Sciences*, 169:382–400.

Ghesmat, K., Hassanzadeh, H., and Abedi, J. (2011). The impact of geochemistry on convective mixing in a gravitationally unstable diffusive boundary layer in porous media: CO_2 storage in saline aquifers. *J. Fluid Mech.*, 673:480–512.

Ginn, T. R. (2001). Stochastic-convective transport with nonlinear reactions and mixing: finite streamtube ensemble formulation for multicomponent reaction systems with intra-streamtube dispersion. *J. Contam. Hydrol.*, 47(1-2):1–28.

Ginn, T. R., Simmons, C. S., and Wood, B. D. (1995). Stochastic-convective transport with nonlinear reaction: Biodegradation with microbial growth. *Water Resour. Res.*, 31(11):2689–2700.

Gouze, P., Melean, Z., Le Borgne, T., Dentz, M., and Carrera, J. (2008). Non-fickian dispersion in porous media explained by heterogeneous microscale matrix diffusion. *Water Resour. Res.*, 44:W11416.

Gramling, C. M., Harvey, C. F., and Meigs, L. C. (2002). Reactive transport in porous media: A comparison of model prediction with laboratory visualization. *Environ. Sci. Technol.*, 36:2508–2514.

Guimerà, J. and Carrera, J. (2000). A comparison of hydraulic and transport parameters measures in low permeability fractured media. *J. Contam. Hydrol.*, 41:261–281.

Gutjahr, A. L., Gelhar, L. W., Bakr, A. A., and MacMillan, J. R. (1978). Stochastic analysis of spatial variability in subsurface flows 2. Evaluation and applications. *Water Resour. Res.*, 14:953–959.

Haggerty, R. and Gorelick, S. M. (1995). Multiple-rate mass transfer for modeling diffusion and surface reactions in media with pore-scale heterogeneity. *Water Resour. Res.*, 31(10):2383–2400.

Hänggi, P., Talkner, P., and Borkovec, M. (1990). Reaction rate theory: fifty years after kramer. *Rev. Mod. Phys.*, 62:251–341.

Hassanizadeh, S. M. and Gray, W. G. (1990). Mechanics and thermodynamics of multiphase flow in porous media including interphase boundaries. *Adv. Water Res.*, 13:169–186.

Hassanzadeh, H., Pooladi-Darvish, M., and Keith, D. W. (2007). Scaling behavior of convective mixing, with application to geological storage of CO2. *AIChE Journal*, 53(5):1121–1131.

Hewitt, D. R., Neufeld, J. A., and Lister, J. R. (2013). Convective shutdown in a porous medium at high Rayleigh number. *J. Fluid Mech.*, 719:551–586.

Hidalgo, J. J. and Carrera, J. (2009). Effect of dispersion on the onset of convection during CO_2 sequestration. *J. Fluid Mech.*, 640:441–452.

Hidalgo, J. J., Fe, J., Cueto-Felgueroso, L., and Juanes, R. (2012). Scaling of convective mixing in porous media. *Phys. Rev. Lett.*, 109:264503.

Hidalgo, J. J., MacMinn, C. W., and Juanes, R. (2013). Dynamics of convective dissolution from a migrating current of carbon dioxide. *Advances in Waer Resoruces*, 62:511–519.

Hornung, U. (1997). *Homogenization and Porous Media*. Springer-Verlag New York, Inc.

Kang, Q., Lichtner, P. C., and Zhang, D. (2006). Lattice Boltzmann pore scale

model for multicomponent reactive transport in porous media. *J. Geophys. Res.*, 111:B05203.

Kapoor, V., Gelhar, L., and Miralles-Wilhelm, F. (1997). Bimolecular second-order reactions in spatially varying flows: Segregation induced scale-dependent transformation rates. *Water Resour. Res.*, 33:527–536.

Kapoor, V. and Kitanidis, P. K. (1998). Concentration fluctuations and dilution in aquifers. *Water Resour. Res.*, 34:1181–1193.

Kazemi, H., Merrill, L., Porterfield, K., and Zeman, P. (1976). Numerical simulation of water-oil flow in naturally fractured reservoirs. *Society of Petroleum Engineers Journal*, 16(6):317–326.

Kechagia, P. E., Tsimpanogiannis, I. N., Yortsos, Y. C., and Lichtner, P. C. (2002). On the upscaling of reaction-transport processes in porous media with fast or finite kinetics. *Chemical Engineering Science*, 57(13):2565 – 2577.

Keller, J. B. (1964). A theorem on the conductivity of a composite medium. *J. Math. Phys.*, 5:548–549.

Kinzelbach, W. (1987). The random walk method in pollutant transport simulation. In Custodio, E., editor, *Advances in analytical and numerical groundwater flow and quality modelling*, volume 224 of *C*, page 227246. NATO ASI.

Kitanidis, P. K. (1988). Prediction by the method of moments of transport in heterogeneous formations. *J. Hydrol.*, 102:453–473.

Kitanidis, P. K. (1994). The concept of the dilution index. *Water Resour. Res.*, 30(7):2011–2026.

Knabner, P., van Duijn, C. J., and Hengst, S. (1995). An analysis of crystal dissolution

fronts in flows through porous media. Part 1: Compatible boundary conditions. *Adv. Water Res.*, 18:171–185.

Kneafsey, T. J. and Pruess, K. (2010). Laboratory flow experiments for visualizing carbon dioxide-induced, density-driven brine convection. *Transp Porous Med*, 82(1):123–139.

LaBolle, E., Fogg, G., and Tompson, A. (1996). Random-walk simulation of transport in heterogeneous porous media: Local mass-conservation problem and implementation methods. *Water Resour. Res.*, 32(2):583–594.

Lallemand-Barres, P. and Peaudecerf, P. (1978). *Recherche des relations entre la valeur de la dispersivité macroscopique d'un milieu aquifer, ses autres caracteristiques et les conditions de mesure*, chapter 3, pages 227–284. Bull BRGM.

Langlo, P. and Espedal, M. (1995). Macrodispersion for two-phase, immiscible flow in porous media. *Advances in Water Resources*, 17:297–316.

Le Borgne, T., Dentz, M., and Carrera, J. (2008). A Lagrangian statistical model for transport in highly heterogeneous velocity fields. *Phys. Rev. Lett.*, 101:090601.

Le Borgne, T., Dentz, M., Davy, P., Bolster, D., Carrera, J., de Dreuzy, J.-R., and Bour, O. (2011). Persistence of incomplete mixing: A key to anomalous transport. *Phys. Rev. E*, 84:015301(R).

Li, L., Peters, C. A., and Celia, M. A. (2006). Upscaling geochemical reaction rates using pore-scale network modeling. *Adv. Water Resour.*, 29.

Li, L., Steefel, C. I., and Yang, L. (2008). Scale dependence of mineral dissolution rates within single pores and fractures. *Geochim. Cosmochim. Acta*, 72:360–377.

Lichtner, P. C. (1985). Continuum model for simultaneous chemical reactions and mass transport in hydrothermal systems. *Geochim. Cosmochim. Acta*, 49:779–800.

Lichtner, P. C. and Kang, Q. (2007). Upscaling pore-scale reactive transport equations using a multiscale continuum formulation. *Water Resour. Res.*, 43:W12S15.

Lichtner, P. C. and Tartakovsky, D. M. (2003). Stochastic analysis of effective rate constant for heterogeneous reactions. *Stochastic Environ. Res. and Risk Assess.*, 17(6):419–429.

Liu, C., Zachara, J. M., Qafoku, N. P., and Wang, Z. (2008). Scale-dependent desorption of uranium from contaminated subsurface sediments. *Water Resour. Res.*, 44:W08413.

MacMinn, C. W. and Juanes, R. (2013). Buoyant currents arrested by convective dissolution. *Geophys. Res. Lett.*, 40(10):2017–2022.

MacQuarrie, K. T. B. and Sudicky, E. A. (1990). Simulation of biodegradable organic contaminants in groundwater: 2. plume behavior in uniform and random flow fields. *Water Resour. Res.*, 26(2):223–239.

Marle, C. M. (1981). *Multiphase Flow in Porous Media*. Editions Technip.

Matheron, G. (1967). Composition des perméabilités en milieu poreux héterogène. Méthode de Schwydler et règles de pondération. *Revue de l'Institute Français du Petrole*, Mars:443–466.

Matheron, M. and de Marsily, G. (1980). Is transport in porous media always diffusive? *Water Resour. Res.*, 16:901–917.

McWorther, D. and Sunada, D. (1990). Exact integral solutions for two-phase flow. *Water Resources Research*, 26:399–413.

Meakin, P. and Tartakovsky, A. M. (2009). Modeling and simulation of pore-scale multiphase fluid flow and reactive transport in fractured and porous media. *Rev. Geophys.*, 47:RG3002.

Meerschaert, M. M., Benson, D. A., Scheffler, H. P., and Becker-Kern, P. (2001). Governing equations and solutions of anomalous random walk limits. *Phys. Rev. E*, 66:060102(R).

Meile, C. and Tuncay, K. (2006). Scale dependence of reaction rates in porous media. *Adv. Water Resour.*, 29:62–71.

Metzler, R. and Klafter, J. (2000). The random walk's guide to anomalous diffusion: a fractional dynamics approach. *Phys. Rep.*, 339(1):1–77.

Mikelic, A., Devigne, V., and Van Duijn, C. J. (2006). Rigorous upscaling of the reactive flow through a pore, under dominant Peclet and Damkohler number. *Siam J. Math. Anal.*, 38:1262–1287.

Molz, F. and Widdowson, M. (1988). Internal inconsistencies in dispersion-dominated models that incorporate chemical and microbial kinetics. *Water Resour. Res.*, 24(4):615–619.

Morales-Casique, E., Neuman, S. P., and Guadagnini, A. (2006). Nonlocal and localized analyses of nonreactive solute transport in bounded randomly heterogeneous porous media: Theoretical framework. *Adv. Water Resour.*, 29(8):1238–1255.

Muskat, M. (1937). *The Flow of Homogeneous Fluids through Porous Media*. McGraw-Hill New York.

Neufeld, J. A., Hesse, M. A., Riaz, A., Hallworth, M. A., Tchelepi, H. A., and Huppert, H. E. (2010). Convective dissolution of carbon dioxide in saline aquifers. *Geophys. Res. Lett.*, 37(22):L22404.

Neuman, S. and Zhang, Y. (1990). A quasi-linear theory of non-fickian and fickian subsurface dispersion 1. theoretical analysis with application to isotropic media. *Water Resour. Res.*, 26(5):887–902.

Neuman, S. P. and Orr, S. (1993). Prediction of steady state flow in non-uniform geologic media by conditional moments: Exact non-local formalism, effective conductivites and weak approximation. *Water Resour. Res.*, 2:341–364.

Neuman, S. P. and Tartakovsky, D. M. (2008). Perspective on theories of anomalous transport in heterogeneous media. *Adv. Water Resour.*

Neuman, S. P., Winter, C. L., and Newman, C. M. (1987). Stochastic-theory of field scale fickian dispersion in anisotropic porous media. *Water Resour. Res*, 23(3):453–466.

Neuweiler, I., Attinger, S., Kinzelbach, W., and King, P. (2003). Large scale mixing for immiscible displacement in heterogenous porous media. *Transport in Porous Media*, 51:287–314.

Noetinger, B., Artus, V., and Ricard, L. (2004). Dynamics of the water-oil front for two-phase, immiscible flow in heterogeneous porous media. 2 isotropic media. *Transp. Porous Media*, 56:305–328.

Nordbotten, J. and Celia, M. (2012). *Geological Storage of CO_2*. John Wiley & Sons.

Panfilov, M. and Floriat, S. (2004). Nonlinear two-phase mixing in heterogeneous porous media. *Transp. Porous Media*, 57:347–375.

Pau, G. S., Bell, J. B., Pruess, K., Almgren, A. S., Lijewski, M. J., and Zhang, K. (2010). High-resolution simulation and characterization of density-driven flow in co_2 storage in saline aquifers. *Advances in Water Resources*, 33(4):443–455.

Pfannkuch, H. O. (1963). *Rev. Inst. Fr. Petr.*, 18:215.

Pope, S. B. (2000). *Turbulent Flows*. Cambridge University Press.

Quintard, M. and Whitaker, S. (1994). Convection, dispersion and interfacial transport of contaminants: Homogeneous media. *Adv. Water Resour.*, 17:221–239.

Rapaka, S., Pawar, R. J., Stauffer, P. H., Zhang, D., and Chen, S. (2009). Onset of convection over a transient base-state in anisotropic and layered porous media. *J. Fluid Mech.*, 641:227.

Rees, D., Selim, A., and Ennis-King, J. (2008). The instability of unsteady boundary layers in porous media. In Vadász, P., editor, *Emerging Topics in Heat and Mass Transfer in Porous Media*, volume 22 of *Theory and Applications of Transport in Porous Media*, pages 85–110. Springer Netherlands.

Renard, P. and de Marsily, G. (1997). Calculating equivalent permeability: a review. *Adv. Water Res.*, 20:253–278.

Rezaei, M., Sanz, E., Raeisi, E., Vázquez-Suñé, E., Ayora, C., and Carrera, J. (2005). Reactive transport modeling of calcite dissolution in the salt water mixing zone. *J. Hydrol.*, 311:282–298.

Riaz, A., Hesse, M., Tchelepi, H. A., and Orr, F. M. (2006). Onset of convection in a. gravitationally unstable diffusive boundary layer in porous media. *J. Fluid Mech.*, 548:87–111.

Risken, H. (1996). *The Fokker-Planck Equation*. Springer Heidelberg New York.

Robinson, B. and Viswanathan, H. (2003). Application of the theory of micromixing to groundwater reactive transport models. *Water Resour. Res.*, 39(11):1313.

Rubin, Y. (2003). *Applied Stochastic Hydrogeology*. Oxford University Press, New York.

Rubin, Y., Sun, A., Maxwell, R., and Bellin, A. (1999). The concept of block-effective macrodispersivity and a unified approach for grid-scale-and plume-scale-dependent transport. *Journal of Fluid Mechanics*, 395:161–180.

Saaltink, M. W., Ayora, C., and Carrera, J. (1998). A mathematical formulation for reactive transport that eliminates mineral concentrations. *Water Resour. Res.*, 34(7):1649–1657.

Sahimi, M. (1995). *Flow and Transport in Porous Media and Fractured Rock*. VCH, Weinheim, Cambridge.

Sahimi, M. (2011). *Flow and Transport in Fractured Media and Porous Rock*. Viley VCH.

Salamon, P., Fernàndez-Garcia, D., and J., G.-H. J. (2006). A review and numerical assessment of the random walk particle tracking methods. *J. Cont. Hydrol.*, 87:277–305.

Sanchez-Vila., X., Dentz, M., and Donado, L. D. (2007). Transport-controlled reaction rates under local non-equilibrium conditions. *Geophyscial Res. Lett.*, 34:L10404.

Sanchez-Vila, X., Guadagnini, A., and Carrera, J. (2006). Representative hydraulic conductivities in saturated groundwater flows. *Rev. Geophys.*, 44:RG3002.

Schmid, K. and Geiger, S. (2012). Universal scaling of spontaneous imbibition for water-wet systems. *Water Resources Research*, 48:W03507.

Schumer, R. D., Benson, M., Meerschaert, M., and Baeumer, B. (2003). Fractal mobile/immobile solute transport. *Phys. Rev. E*, 39(10):1296.

Seeboonruang, U. and Ginn, T. R. (2006a). Upscaling heterogeneity in aquifer reactivity via exposure-time concept: Forward model. *J. Cont. Hydrol.*, 84:127–154.

Seeboonruang, U. and Ginn, T. R. (2006b). Upscaling heterogeneity in aquifer reactivity via the exposure-time concept: Inverse model. *J. Cont. Hydrol.*, 84:155–177.

Simunek, J., Jarvis, N. J., van Genuchten, M. T., and Gärdenäs, A. (2003). Review and comparison of models for describing non-equilibrium and preferential flow and transport in the vadose zone. *Journal of Hydrology*, 272:14–35.

Slim, A. C., Bandi, M. M., Miller, J. C., and Mahadevan, L. (2013). Dissolution-driven convection in a hele-shaw cell. *Physics of Fluids*, 25(2):024101.

Slim, A. C. and Ramakrishnan, T. S. (2010). Onset and cessation of time-dependent, dissolution-driven convection in porous media. *Physics of Fluids*, 22(12):124103.

Steefel, C. I., DePaolo, D. J., and Lichtner, P. C. (2005). Reactive transport modeling: An essential tool and a new research approach for the earth sciences. *Earth and Planetary Science Letters*, 240:539–558.

Steefel, C. I. and MacQuarrie, K. T. B. (1996). Approaches to modeling reactive transport. In *Reactive Transport in Porous Media*, volume 34, pages 83–129. Mineral Soc. of Am.

Szulczewski, M. L., Hesse, M. A., and Juanes, R. (2013). Carbon dioxide dissolution in structural and stratigraphic traps. *J. Fluid Mech.*, 736:287–315.

Tartakovsky, A. M., Meakin, P., Scheibe, T. D., and Eichler-West, R. M. (2007). Simulations of reactive transport and precipitation with smoothed particle hydrodynamics. *J. Comp. Phys.*, 222:654–672.

Tartakovsky, A. M., Redden, G., Lichtner, P. C., Scheibe, T. D., and Meakin, P. (2008). Mixing-induced precipitation: Experimental study and multiscale numerical analysis. *Water Resour. Res.*, 44:W06S04.

Tartakovsky, A. M., Tartakovsky, G. D., and Scheibe, T. D. (2009). Effects of incomplete mixing on multicomponent reactive transport. *Adv. Water Resour.*, 32:1674–1679,.

Tecklenburg, J., Neuweiler, I., M., D., Carrera, J., Geiger, S., Abramowski, C., and Silva, O. (2013). A non-local two-phase flow model for immiscible displacement in highly heterogeneous porous media and its parametrization. *Adv. Water Resour.*, 62:475–487.

Tilton, N., Daniel, D., and Riaz, A. (2013). The initial transient period of gravitationally unstable diffusive boundary layers developing in porous media. *Physics of Fluids*, 25(9):092107.

Villermaux, J. and Devillon, J. C. (1972). Représentation de la coalescence et de la redispersion des domaines de ségrégation dans un fluide par un modèle d'interaction phénom- enologique. In *Proc. 2nd International Symposium Chem. React. Engineering, New York, Elsevier.*

Wen, X.-H. and Gómez-Hernández, J. J. (1996). Upscaling hydraulic conductivities in heterogeneous media: An overview. *J. Hydrol.*, 183:9–23.

West, B. J., Bologna, M., and Grigolino, P. (2003). *Physics of Fractal Operators*. Springer New York Berlin Heidelberg.

Whitaker, S. (1986). Flow in porous media I: a theoretical derivation of Darcy's law. *Trans. Porous Media*, 1:3–25.

Whitaker, S. (1999). *The Method of Volume Averaging*. Kluwer Academic Publishers.

White, A. F. and Peterson, M. L. (1990). *Chemical Modeling of Aqueous Systems II*, chapter Role of Reactive-Surface-Area Characterization in Geochemical Kinetic Models, pages 461–475. American Chemical Society.

Willingham, T. W., Werth, C., and Valocchi, A. J. (2008). Evaluation of the effect of media structure on mixing-controlled reactions using pore-scale modeling and micromodel experiments. *Environ. Sci. Technol.*, 42:3185–3193.

Willmann, M., Carrera, J., and Sanchez-Vila, X. (2008). Transport upscaling in heterogeneous aquifers: What physical parameters control memory functions? *Water Resour. Res.*, 44:W12437.

Willmann, M., Carrera, J., Sanchez-Vila, X., Silva, O., and Dentz, M. (2010). Coupling of mass transfer and reactive transport for non-linear reactions in heterogeneous media,. *Water Resour. Res.*, page doi:10.1029/2009WR00773.

Winter, C. L., Tartakovsky, D. M., and Guadagnini, A. (2003). Moment differential equations for flow in highly heterogeneous porous media. *Surv. Geophys.*, 24:81–106.

Wyckoff, R. D. and Botset, H. G. (1936). The flow of gas liquid mixtures through unconsolidated sands. *J. Appl. Phys.*, 7:325–345.

Xu, X., Chen, S., and Zhang, D. (2006). Convective stability analysis of the long-term storage of carbon dioxide in deep saline aquifers. *Advances in Water Resources*, 29(3):397–407.

Yang, Z., Niemi, A., Fagerlund, F., and Tissa Illangasekare, T. (2013). Two-phase flow in rough-walled fractures: Comparison of continuum and invasion-percolation models. *Water Resour. Res.*, 49:993–1002.

Zhang, D. and Tchelepi, H. (1999). Stochastic analysis of immiscible two-phase flow in heterogeneous media. *SPE Journal*, 4:380–388.